Chapter 5:

Description of MCM-41 Structure

"If it were possible to bore parallel cylindrical holes through solid silica, a series of samples with holes of different sizes could be made while keeping a constant pore volume per gram of silica. . . Since all the pores are the same size, they would all fill at once when a certain vapour pressure is reached. Also, since the pores are of uniform size, no hysteresis should be observed. . . This idealised situation, of course, does not occur in actual silica gels. . . "

Ralph K. Iler, The Chemistry of Silica, p491.

MCM-41 is often proposed as a model mesoporous adsorbent, the perfect material for comparison between experiment and theory in the adsorption field.[1-3] The characteristics of MCM-41 cited as making it a model adsorbent are[4] (1) it consists of an array of uniform hexagonal channels of tuneable size, (2) the pore length is significantly greater than the pore diameter (3) the absence of pore channel intersections guarantees that pore networking effects are negligibly small and (4) X-ray diffraction can provide an independent estimate of pore sizes. The work described in this chapter throws doubt on at least one of the first three characteristics, and suggests that the quality of most published diffraction patterns is insufficient to develop a detailed model for MCM-41. The other significant proposed application of MCM-41, as an inert, high surface area substrate for catalytic applications, which often involves attachment of active molecules to the inner pore surfaces, would also benefit from a more detailed model of the wall structure. This would clarify the mode of attachment and subsequent activity of the guest molecules.

The structure of MCM-41 has for the most part, been assumed to consist of amorphous silica of density similar to that of colloidal silicas,[5,6] pierced by large holes which do not greatly perturb the wall structure. This simple model of the structure has not been verified because of the small number of peaks in the MCM-41 X-ray diffraction patterns. Patterns showing only three or four broad peaks, which are the norm in published literature, do not contain sufficient information about the channel arrangement to allow detailed modelling of the wall structure. The width of these diffraction peaks, and the fact that it has been possible to improve the number and sharpness of visible diffraction peaks from MCM-41 by various preparative methods,

indicate that the channels of these four-peak materials are not very well ordered. Nitrogen isotherm measurements have shown that no micropores are present in the structure,[7] but make no further conclusions concerning the nature of the walls. With the improvements to the preparation reported in Chapter 4, it has been possible to gain more information from the diffraction patterns of the MCM-41 materials and so to propose a structural model which is much more detailed than those previously reported.

5.1 Introduction

As discussed in Chapter 3, the characterisation of MCM-41 in this work is performed using several techniques. Given the mesoscale size range of the structure, small angle scattering and small angle diffraction techniques have been most useful in determining the detailed structure of the material. The model derived from X-ray diffraction is supported by neutron diffraction measurements on adsorbed hydrogen. The results from small angle neutron scattering contrast variation experiments are also compatible with the proposed model.

As mentioned above, the small number of X-ray diffraction peaks from MCM-41 in most published reports has made the determination of a detailed wall structure for this material difficult. Work on MCM-41 wall structure has concentrated on experimental measurements of various types. Most commonly, wall thicknesses are calculated using a combination of nitrogen or argon adsorption isotherms and X-ray data. The thickness is found by subtracting the pore diameter found from the adsorption isotherm from the centre to centre distance of the cylindrical pores found from the X-ray *d*-spacing.[8-15] This method implicitly assumes smooth walled mesopores, since the calculation of pore diameters from adsorption isotherms assumes an absence of micropores.[16]

Pore dimensions have also been calculated using ^{1}H nmr measurements of the phase transitions of water in the MCM-41 channels. These were however, calibrated against nitrogen adsorption isotherms and electron micrograph measurements.[17] In that work a factor is included in the pore radius to achieve agreement with nitrogen isotherm measurements. It is ascribed to a non-freezing layer of water on the pore surface which acts physically as the pore wall reducing the effective, observed pore radius, analogous to the multilayer thickness factor in pore size determination from nitrogen adsorption isotherms. Wall thicknesses are also calculated from through focus high resolution electron microscopy (HREM) photographs with minimum wall thicknesses found to be around 8 Å[18] but higher values also often quoted (10-13 Å).[18,19] The larger values are often explained as being edge or angled views of the wall structure. Some evidence for wall roughness and the presence of amorphous material in the MCM-41 pores has also been found using this technique, and is supported by thermoporimetry on adsorbed water.[20]

Some modelling work has been carried out. A molecular dynamics simulation by Feuston and Higgins[6] used an empirical interaction potential for vitreous silica in a model which contained fixed pores of diameter 39.6 Å, and filled the interstitial spaces with various thicknesses of silica, or kept the lattice constant fixed at 44.6 Å, while

varying the wall thicknesses between 5.9 Å and 10.9 Å. Silica was placed into the structure with a density close to that of vitreous silica and annealed. Atoms were added to ensure most silicon atoms were bound to four oxygens. These simulations resulted in structures with a predominance of 4 and 5-fold siloxane rings whereas experimental results have shown a high proportion of 3-fold[5] and 4-fold[21] siloxane rings. Diffraction patterns calculated from this work show up to four peaks, with the thickest wall structure simulated (11 Å) giving the best correspondence with experiment.

Another theoretical calculation using Monte Carlo methods tried to simulate the nitrogen adsorption isotherms obtained for MCM-41.[22] Again, a smooth pore appears to have been implicitly assumed, with the oxygen atom radius taken from studies of silicalite. The interaction parameter between nitrogen and an MCM-41 oxygen was found by fitting simulated isotherms to experimental results. The results of this simulation suggest that the shape of experimental isotherms indicate the presence of pores which are not monodisperse, and the presence of some micropores (diameter < 2 nm). The situation contrasts with that for buckytubes in which good agreement between experiment and calculations was found. Another study of adsorption isotherms modelled the MCM-41 as smooth cylinders between energetically homogeneous walls 10(3) Å thick.[4] Their predicted isotherms followed the stepwise behaviour of the observed nitrogen adsorption isotherm, but the work showed that a more detailed model of the MCM-41 wall was necessary, to account for the energetic heterogeneity observed in this material.

Beck *et al.*[8] fit X-ray diffraction data containing four peaks using models based both on a hexagonal three-dimensional tetrahedral framework and on hexagonal arrays of cylindrical shells with walls having a continuous distribution of scattering matter. They concluded that any model with a hexagonal array of cylindrical pores and thin walls will exhibit similar patterns, so that diffraction intensities were of limited use in structure determination. Stucky *et al.*[23] report briefly a structure based on fitting of diffraction data containing five to six peaks from the MCM-41 hexagonally packed channel array. They used a model which assumed an amorphous continuous scatterer for the walls, with a periodic array of void tubes. Two parameters were refined, the wall thickness and the pore shape, by using analytically derived functions to describe hexagonal and cylindrical geometries as wall shape functions. They found a best fit for walls 8(1) Å thick for unit cells between 37.5 - 46.9 Å and hexagonal shaped pores. This gave void space fractions of 0.6-0.7 which compared to experimental measurements of 0.62 - 0.74, for argon and nitrogen adsorption measurements.

Other simulations have been performed for the mesoporous silicate FSM-16 using X-ray diffraction (XRD) data containing four peaks, nitrogen adsorption data and transmission electron micrographs.[24] This material has similar pore dimensions to MCM-41 but is synthesised by intercalation of quaternary ammonium surfactants into a layered silicate (kanemite) and there is some debate over whether FSM-16 and MCM-41 are the same material.[18,25] In this study by Inagaki *et al.*[24] the uncalcined materials were found to have pore walls 4 Å thick with a pore diameter of 42 Å, while the calcined materials contained walls 8 - 9 Å thick with pore diameters of 34-37 Å. These were in good agreement with nitrogen isotherm measurements (pore diameters

27-35 Å , wall thickness 16 Å, for the calcined material) and transmission electron micrographs (pore diameter 31 Å, wall thickness 12 Å) for the same materials. The XRD intensity profile was fitted for a hexagonal arrangement of infinitely long cylinders, allowing for hexagonal symmetry by allowing overlap between neighbouring rods. Inagaki and co-workers[24] propose that the walls are made up of a single, or double layer of silica tetrahedra, with the pore shrinkage caused by the degree of wrinkling of the silicate layers. The uncalcined material would have stretched walls, due to the large surfactant cations attached to the walls, while the calcined materials would have strongly wrinkled walls due to the removal of the large cations. This would allow the surface to buckle, and then condense during calcination to form the observed thicker walls. They also acknowledge that this mechanism does not fully account for the observed thickness change.

A study by Ortlam *et al.*[26] calculated pore size by assuming it to be dependent upon the size of the template micelles. This is determined by the packing parameter *v/al* where *v* is the volume of the hydrocarbon chain, *a* the headgroup area and *l* the maximum effective chain length (somewhat less than the fully extended molecular length of the chain). For cylindrical micelles, $1/3<v/al<1/2$. The parameter, *a*, is known to be sensitive to the surfactant counterion, and for silicate species used in that work, was taken to be 0.63 nm^2. The volume and length of the hydrocarbon chain were taken from previous work on surfactants. The mean micelle diameter thus calculated was then assumed to be the pore diameter. A relationship between pore volume, pore diameter, wall density and wall thickness was then derived, wherein a wall density of 2.3 g cm^{-3}, typical of non-porous aluminosilicates was assumed. This relationship was used along with pore diameters from nitrogen adsorption isotherms and unit cell measurements from XRD to calculate experimental wall thicknesses which ranged from 9 to 12 Å. The calculated micelle diameters and pore volumes (assuming wall thicknesses of 8 - 10 Å) gave reasonable agreement with experiment. Calculating back from their experimental results, however, gave a wall density for silica of 1.8 g cm^{-3} and substitution of the density of the MCM-41 walls found in this work (below) resulted in wall thicknesses of around 20 Å, close to those calculated from the X-ray modelling discussed below. This model is, therefore not inconsistent with the structure derived in this work.

5.2 Macroscopic Structure

The morphology of the MCM-41 crystallites has been discussed in Chapter 4 (see the scanning electron micrographs in Figures 4.25, 4.26). No evidence of regular hexagonal crystallites, as seen by other workers,[8,27] was found in this work for either the ordinary preparation materials, or the more highly ordered materials from the acid-titrated preparations. For the materials with greater long range order, scanning electron micrographs show smooth, rounded particles, with frequent, large scale wormlike protrusions, but no evidence of spheres or any other regular shape (see Figures 4.30, 4.31). Transmission electron microscopy (shown in Figures 4.27, 4.28) suggests that the MCM-41 particles consist of bundles of tubes packed in a fairly ordered manner, which then agglomerate with other such bundles, forming the larger particles. Scherrer

analysis of the peak widths from small angle diffraction patterns gives coherence lengths of the order of 1000 - 2000 Å. This corresponds to the size of the large wormlike agglomerations, and curled tubes imaged in the TEM. No further ordering on a macroscopic scale was observed for the materials studied in this work, although other workers have prepared mesoporous spheres with millimetre dimensions,[28] patterned silicate structures resembling diatoms[29] and other very large scale (200 nm--0.5 μm) structures.[30] Monoliths of silica/surfactant composites in the hexagonal, cubic and lamellar phases have also been prepared,[31] with dimensions governed by those of the container in which they were made.

5.3 Mesoscopic Structure

The silicate in MCM-41 surrounds hollow tubes, which are arranged in a relatively regular two dimensional hexagonal array. The material appears otherwise to be amorphous. There is considerable interest in improving the order of the channel array in the final product and in discovering the structure of the walls of the tubes, and their detailed arrangement. Improved X-ray diffraction experiments are one straightforward way to validate more detailed models. Some work on diffraction studies has been reported previously and is described above. The results of the optimised synthetic work described in Chapter 4 allow a more detailed analysis using seven diffraction peaks, and this, combined with data from small angle neutron scattering, and neutron diffraction on hydrogen adsorbed in MCM-41 has resulted in a more detailed model of the wall structure. Quasielastic and inelastic neutron scattering studies of molecules adsorbed in MCM-41, which are described in Chapter 6, provide further support for this model.

5.3.1 Synchrotron X-Ray Study

5.3.1.1 Background

Chapter 4 describes the optimisation of the MCM-41 synthesis. Heating of a CTAB/silicate gel system for periods of about three days at 100˚C, produces a material with X-ray diffraction patterns showing two or three orders of the in-plane (35 Å) *d*-spacing.[32] An improvement to this method was reported by Ryoo and Kim,[33] who took account of the fact that during the synthesis the pH of the system generally rises, and that this might well be inimical to the crystallisation process. Further optimisation of this synthesis by monitoring the observed number of orders of the X-ray diffraction and the intensities of the peaks is reported in Chapter 4 and resulted in materials having in-plane *d*-spacings of around 44 Å. The centre-to-centre distance between the hexagonally arranged channels in the MCM 41 matrix is equal to $2/\sqrt{3}$ times the *d*-spacing from X-ray diffraction patterns for this material.

The synthesis gels for the materials studied using synchrotron X-rays were made up as described in Chapter 4 and were titrated during synthesis with one molar sulphuric or acetic acid to maintain the pH of the reaction mixture at 11, while heating at 100˚C was carried out for 4 days. The molar composition of the synthesis gels were typically 1.00 CTAB/ 1.89 SiO_2/ 0.738 Na_2O/ 0.267 H_2SO_4/ 0.123 HX/ 160 H_2O, where HX is the

acid used as titre in each case. The MCM-41 materials were calcined in a muffle furnace at 500˚C overnight. The sulphuric acid treated samples were from the same preparation, but were calcined at two different times and are labelled (1) and (2), with (2) having been calcined several months later than (1). Nitrogen isotherms at 77 K were obtained from the calcined samples using a Sartorius microbalance, to determine the surface areas. The BET surface areas were 990 $m^2\ g^{-1}$ for material titrated with sulphuric acid, and 750 $m^2\ g^{-1}$ for the material titrated with acetic acid. Nitrogen adsorption isotherms are discussed in more detail in Chapter 6, section 6.8.

5.3.1.2 Results and Discussion

Figure 5.1 shows the patterns obtained from uncalcined and calcined specimens produced by titration with sulphuric acid during synthesis. This is the most highly ordered material obtained so far. Peak areas, on an arbitrary but constant scale, and *d*-spacings, indexed on a two dimensional hexagonal lattice, for calcined and uncalcined samples from preparations titrated with sulphuric and acetic acids are given in Tables 5.1 and 5.2 below.

Table 5.1 *Observed x-ray intensities after background fitting and subtraction, from template containing and calcined MCM-41, produced from sulphuric acid and acetic acid controlled pH synthesis conditions.*

Reflection	Sample				
	H_2SO_4 (1) Calcined	H_2SO_4 (2) Calcined	H_2SO_4 Uncalcined	CH_3COOH Calcined	CH_3COOH Uncalcined
(10)	26.683	*	10.082	*	6.574
(11)	6.576	5.536	1.637	5.536	1.156
(20)	4.465	3.984	1.335	4.317	0.894
(21)	2.436	2.595	1.245	2.249	0.813
(30)	0.124	0.162	0.119	0.171	-
(22)	0.030	0.087	0.059	0.069	-
(31)	0.141	0.187	0.065	0.171	-

Note: * Peaks which had their tops cut off in the process of data extraction.
- Peaks at these positions had no visible intensity.

On removing the template by calcination there is a contraction in the average *d*-spacing from *ca.* 42 Å to 39 Å. This may increase the density of the walls, increasing the X-ray contrast between walls and channels. In addition, removal of the channel contents, template, and perhaps some water, will also increase this contrast. The effect of this change in contrast can be seen in the much higher intensities obtained for calcined specimens in Table 5.1 compared with the uncalcined ones.

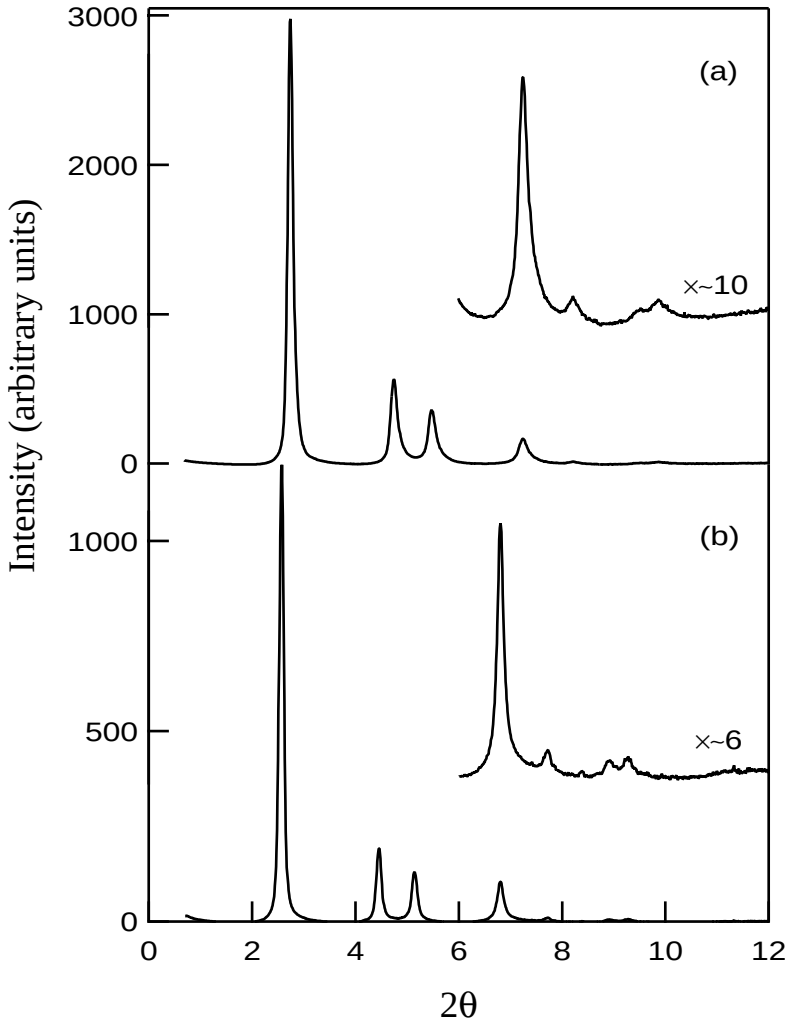

Figure 5.1 *Synchrotron X-ray diffraction patterns for (a) calcined and (b) uncalcined materials titrated against H_2SO_4 to maintain a pH of 11 during synthesis. The last four peaks for each trace, magnified by the factors shown, are inset.*

The data from Figure 5.1 also allow a form factor to be fitted. The natural small angle scattering form factor for such a tubular system is that for a hexagonal array of cylinders.[34] It is reasonable to modify this form factor by a Debye-Waller factor, to take account of thermal motion, and the variability of both tube centre position and tube internal diameter. However, this form factor convoluted with the Debye-Waller factor oscillates strongly in Q space, with sharp decreases to zero, which are not observed. The observed intensities do however change sharply in intensity at Q *ca.* 0.5 $Å^{-1}$ (see for example Figure 5.2), as does the cylinder function for tubes of the expected diameter of *ca.* 20 Å. The data, besides the problem of the zeros, also fit extremely poorly to a single channel model.

To remove these unobserved zeros, a second cylinder of different density to both the walls and the hole, whose form factor 'interferes' with the first, was inserted into the model. Physically this means that the wall structure will be described as concentric cylinders of different contrast density, one of which is slightly smeared by a Gaussian to smooth the interface between them. Thus there is a connected region of denser silica

forming the walls between cylinders, cylindrical regions of less dense silica filling some of the volume within the dense boundary layers, and finally the empty (or surfactant filled, in the case of the uncalcined materials) channels in the centres of the tubes. The equation used to approximate the Bragg intensities is :-

$$A(Q) = \left(\frac{2K_1}{R_1 Q} J_1(Q, R_1) + \frac{2K_2}{R_2 Q} J_1(Q, R_2) e^{-\alpha Q^2}\right)^2 \qquad \textbf{(5.1)}$$

where A is the area under the peak, Q is momentum transfer, R_1 is the radius of the outer cylinder, R_2 is the radius of the inner cylinder, K_1 and K_2 are constants related to the scattering length densities of each region, $J_1(Q,R)$ is the first order Bessel function and α is a Debye-Waller constant. The radii, R_1, R_2, and the constants, K_1, K_2, were parameters in the fit, and α was set to 1.0 Å^2 since varying this parameter did not alter the fit significantly, provided it was kept small.

The fit was carried out using a least squares method, maintaining consistency across the five data sets. This method minimises χ^2, starting from a variety of physically possible values of K_1, K_2, R_1 and R_2. The fit is stable to a wide choice of initial values. In the two cylinder model, introduction of further smearing, via a second α on R_1, does not improve the fit. Figure 5.2 shows a typical fit to a set of data points (for calcined material titrated against sulphuric acid during preparation). Four extra points with zero intensity were added to the data for fitting purposes. These corresponded to Q values where hexagonal peaks for the 32, 33, 41 and 42 reflections would be expected, but which were not observed.

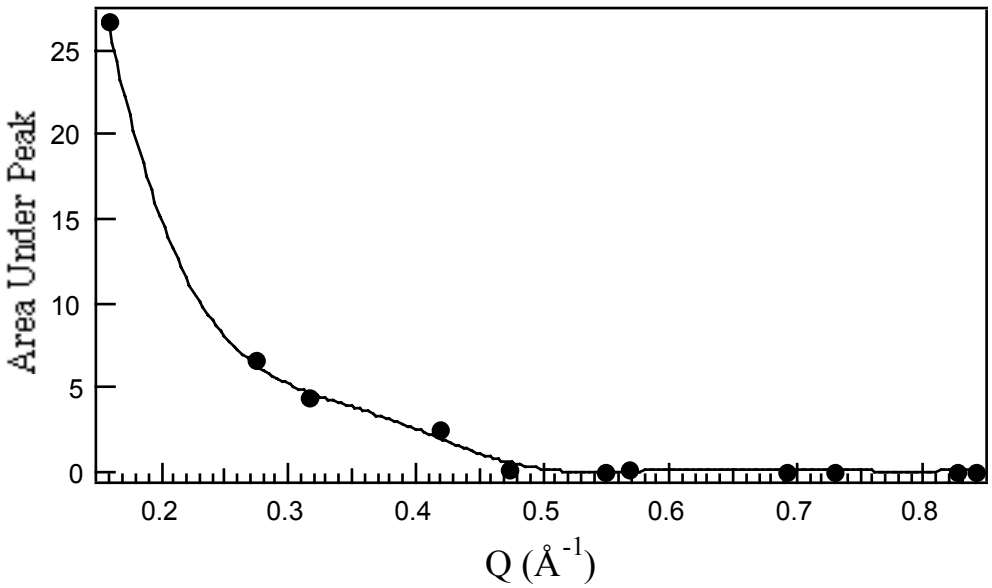

Figure 5.2 *Area under the peak plotted against Q for calcined MCM-41 titrated against sulphuric acid to maintain a pH of 11 during preparation, and the model fit to the data.*

An attempt was made to distinguish between cylindrical and hexagonal shaped large and small pores, following the report of Stucky *et al.* that hexagonal pores were a better fit to their data.[23] Substituting a numerically calculated form factor for a hexagonal

cross-section instead of a circular one, of identical cross-sectional area, resulted in no improvement in the fit and there was no experimental reason to choose one over the other. The change from circular to hexagonal is of the order of ±1 Å in the 20 Å radius. The highest order reflection was observed to be at a *d*-spacing of ~11 Å, giving a resolution of *ca.* 7 Å, which, in itself indicates that such detailed shape information is not available from this data.

Parameter values for the best fit to the data for both the calcined and uncalcined materials are shown in Table 5.2, which also gives the derived minimum wall thicknesses. The features of this model can be summarised as a cylindrical hole of radius R_2, *ca.* 7 Å surrounded by a ring of material of thickness *ca.* 13 Å, of noticeably reduced density from the wall density. The boundary between the hollow core and low density silica region is quite sharp, although the boundary between lower and higher density silicate regions is less so. The requirement for three regions in MCM-41 - hole, intermediate region of significantly reduced density, and wall, is the major conclusion (see Figure 5.3). A two region hole/wall model is not adequate.

Table 5.2 *Lattice parameters measured from SAXS data and fit parameters from iterative fits of the form factors for synchrotron X-ray data from calcined and uncalcined MCM-41 produced from sulphuric acid and acetic acid controlled pH synthesis conditions.*

Fit Parameters	Sample				
	H_2SO_4 (1) Calcined	H_2SO_4 (2) Calcined	H_2SO_4 Uncalcined	CH_3COOH Calcined	CH_3COOH Uncalcined
R_1 / Å	19.69(5)	19.61(5)	21.42(5)	20.18(5)	20.82(5)
R_2 / Å	6.89(5)	7.40(5)	7.02(5)	7.34(5)	6.75(5)
K_1	3.95(5)	7.91(5)	4.18(5)	6.71(5)	3.01(5)
K_2	5.31(5)	6.39(5)	2.92(5)	5.94(5)	2.31(5)
d-spacing / Å	39.64(2)	38.7(1)	42.23(2)	39.9(1)	42.31(2)
centre to centre distance, $2R_3$ / Å	45.77(2)	44.7(1)	48.76(2)	46.1(1)	48.86(2)
dense wall thickness / Å	6.39(5)	5.5(4)	5.92(5)	5.7(4)	7.22(5)
less dense wall thickness / Å	12.80(7)	12.2(7)	14.40(7)	12.8(7)	14.07(7)
total wall thickness per micelle / Å	16.00(5)	15.0(8)	17.36(5)	15.7(8)	17.68(5)

The X-ray data gives a projection of the three dimensional structure onto the hexagonal lattice plane. Thus the radii of the various regions are averages of the structures at various heights in the channels. The radius of the central hole could be somewhat larger than stated, if it had some variation in its centre point. Such a variability of the hole would contribute to the apparently lower density observed in the inner region with reduced silicate density. However the sharpness of the hole boundary, reflected in the low value of α, suggests this is not likely. It should be noted that the three-region model proposed here is the simplest model involving variable silica densities in the wall and lining regions. A model with a small central hole and some smoothly varying continuous silica density in the walls (as shown in Figure 5.3) would also fit the data.

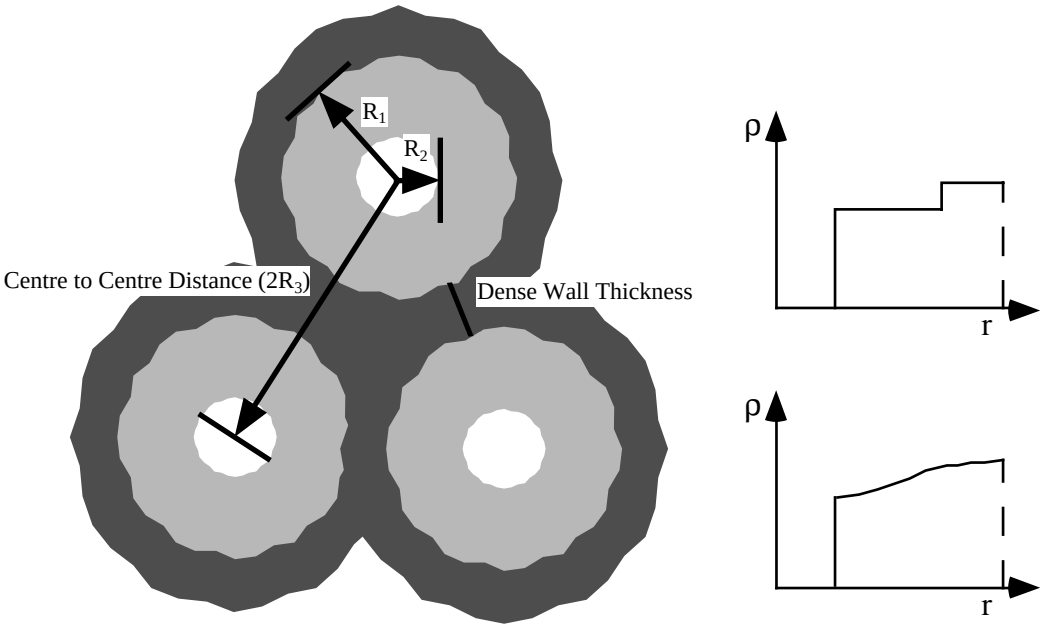

Figure 5.3 *Schematic diagram of the proposed model for MCM-41 (left) with two possible density distributions for the silica in the walls (right). The model discussed in detail here corresponds to the top distribution which is the simplest model for introducing variable silica density into the wall/lining region. The bottom distribution would also fit the data.*

The calcined MCM-41 from the preparation titrated against acetic acid has a slightly thinner dense wall at 5.7(4) Å, than the similarly calcined sulphuric acid sample at 6.4(1) Å, but in the uncalcined materials the trend is reversed, with dense walls of 5.9(1) Å for the sulphuric acid treated, and 7.2(1) Å for the acetic acid treated materials respectively. The minimum thicknesses obtained for the dense parts of the walls for the calcined materials are smaller than those estimated from previous fitting of less extensive X-ray data, (8 Å),[8,23] high resolution electron microscopy (8 - 13 Å)[18,35] and combined analysis of nitrogen adsorption isotherms and X-ray diffraction data (12.5 Å).[10,19,36] The average values obtained for the total wall thicknesses however, 15.6(3) Å, for the calcined and 17.5(2) Å for the uncalcined materials are much larger than those earlier estimates. These earlier methods measured only an average wall thickness, since they assume a simple two region hole/wall model.

In the calcined materials the less dense silicate layer has a thickness of around 12.6(2) Å, whereas in the uncalcined materials it is about 14.2(2) Å. This contraction from uncalcined to calcined materials appears to be the major contribution to the decrease in the *d*-spacing after calcination, since the dense wall thicknesses, and the hole radii appear to remain roughly constant at 6 and 7 Å respectively. As this region has a lower silicate density than the outer walls it is reasonable to assume that upon calcination, as water trapped in the walls and the charged surfactant supporting the first layer of silicates are removed, there will be a further condensation and relaxation of the silicate groups, resulting in a slight increase in density and decrease in thickness of this layer. In FSM-16, a material with a similar hexagonal channel structure, (discussed above in section 5.1) such a contraction with calcination is ascribed to the buckling of the stretched layer of silica tetrahedra forming the walls into a wrinkled configuration upon removal of the large, supporting template ions. The collapse into the wrinkled layer which then condenses is at least partially responsible for the increase in wall thickness.[24] It was also suggested that silicates remaining in solution in the FSM-16 channels even after drying are deposited on the walls during calcination, stabilising and thickening them.[24] Presumably, in MCM-41 materials not titrated with acid during synthesis, where a larger contraction occurs during calcination, this collapse would be more obvious in the X-ray data, although this material does not show enough diffraction peaks to allow useful modelling.

If the thicknesses of the dense and less dense contributions to the walls are summed, then the uncalcined 'walls' are thicker (17.5(2) Å) than those of the calcined materials (15.6(3) Å) by a couple of angstroms. This is largely due to the thicker porous layer discussed above. These overall wall thicknesses are larger than those found in earlier work,[8,10,19,23] for materials prepared using the ordinary alkaline synthesis method. Some work on the effect of the initial pH of the alkaline synthesis gel on wall thickness has found that the thickness increases with decreasing pH up to 16 Å, suggesting a thicker silicate coat is deposited on the micelles as the silica solubility decreases.[37] However none of these earlier results used preparations adjusted for pH *during* synthesis. From the work reported in Chapter 4, these acid titrated materials, appear to be much more hydrothermally stable than those from the ordinary MCM-41 preparation and so may well have thicker or more densely polymerised walls to achieve this stability. Other work using neutral surfactant templates and silicates indicates the existence of thicker walls in those materials[9,11] even though in that case there is a decrease in overall crystallinity. Wall thicknesses of up to 27 Å have been reported for an optimised ordinary MCM-41 synthesis.[14] Those thick walled materials showed greater hydrothermal stability and slightly lower surface areas than thinner walled samples, as are seen for the acid-titrated materials in this work. Thicker walls in these acid titrated materials are therefore not improbable and are possibly reflected in the slightly lower surface BET surface areas found for these materials compared to the less well ordered samples (see Chapter 4).

The constants, K_1 and K_2 in the fits are proportional to the relative scattering length densities in different parts of the structure. Ratios of these numbers, combined with other experimental information can be used to calculate the absolute densities of the walls. In the calcined material, the high surface areas given by the nitrogen isotherms

indicate that there is nothing left in the central hole, and so its density may be set to zero. Also from the nitrogen isotherms of this calcined material, the large volume of nitrogen adsorbed (0.8 $cm^3\ g^{-1}$) allows the mean density of MCM-41 to be calculated at around 0.83(5) g cm^{-3}, assuming a bulk density for silica at 2.5 g cm^{-3}. This is comparable to the particle density of a silica gel formed from a sodium silicate solution at a pH of 9.5, which has been measured to be 0.86 g cm^{-3}.[38] Other workers[39] have measured the mean density of calcined boron-substituted MCM-41 materials to be 0.97(4) g cm^{-3}, in reasonable agreement with the result above. The silicate skeleton in that work was found to have a density of 2.2(1) g cm^{-3}, with the remainder being void space. For the uncalcined materials, the void space will be filled with the template, CTAB, and residual water, so the mean density of the uncalcined material (assuming roughly the same amount of void space as in the calcined material) will be about 1.50(5) g cm^{-3}. These numbers, and the relative volumes of the regions derived from the X-ray model, give the densities of different parts of the structure, by solving simultaneous equations for the relative scattering length densities of various parts of the structure.

In the calcined material, the density of the walls is 0.99 g cm^{-3}, less than half that of amorphous silica, the porous region of the calcined material is 0.87 g cm^{-3}. This corresponds to 60% void space in the dense wall of the calcined materials, and 65% in the less dense wall. While the absolute values given here have errors estimated at 4-5%, the difference has an error of less than 1%. In the uncalcined materials, the denser part of the wall has a density of 1.57 g cm^{-3}, the less dense wall has a density of 1.51 g cm^{-3} and the hole is filled with material having a density of 1.09 g cm^{-3}. This latter value agrees with a theoretical CTAB or water density, and increases confidence in the reality of the model. The wall densities are higher in the uncalcined material since the void space in this material is filled with water and template. The void space in the dense wall of the uncalcined material must therefore be 62%, and in the less dense wall 66%, which is approximately the same as that in the calcined material. There is clearly very little silica in the MCM-41 structure, when compared to the volume enclosed, implying rough, highly-divided “walls”. Attempts to model these density variations by fluctuations in a smooth walled channel diameter required very unlikely distributions. As the difference between the densities of the denser walls and the linings is only about 5%, any fluctuation in a smooth wall would require long stretches of material with the same density as the dense walls, separated by very narrow indentations containing no silica - a "beads on a string" shaped channel space, which was mostly comprised of "string".

Some evidence for roughness in the walls of MCM-41 has been found by through-focus exit wave reconstruction of TEM micrographs of material with a hexagonal morphology.[20] Also observed using this method was the presence of amorphous material inside the pores. Other experimental results on this system , such as small angle neutron scattering and inelastic neutron scattering, discussed below, also point towards this highly porous, three region structure. Other workers have also found evidence for occluded water in the walls of MCM-41.[40] Ion-exchange of Cu(II) ions into Al-MCM-41 has been found to occur on sites which are situated inside the walls of the Al-MCM-41 structure, since they are inaccessible to bulky adsorbate molecules.[41] This is also strongly suggestive of a highly porous wall structure. Low-temperature

phase transitions have been observed in water adsorbed in MCM-41 pores studied using proton nmr.[42] Such transitions have been previously ascribed to the freezing of water in micropores, and one study found that the fraction of water involved in such transitions in MCM-41 implies that more than 60% of the pore volume is related to micropores.[42] In that case, since N_2 adsorption had shown an insignificant amount of microporosity in the samples used in that study, the unfreezing water phase was instead attributed to a layer of thickness 5.4±1.0 Å between the walls and the central channel filled with ice. That work notes that this thickness is of the same order as the dimensions of micropores (0-10 Å), however, observes that the temperature of the phase transition of this interfacial water is significantly higher in mesoporous systems than in solely microporous systems. It is possible that the porous nature of the walls found in this work may be an alternate explanation for their observations, since no evidence of micropores is found from the nitrogen adsorption isotherms for this material either.

5.3.2 Neutron Diffraction Study

5.3.2.1 Background

The behaviour of adsorbed gases on MCM-41 has been studied for many gases. Some of the molecules studied include methane,[43] hydrogen,[44] nitrogen,[2,4,45,46] argon,[7,15] cyclohexane,[18,19] cyclopentane,[47] benzene[8] and water.[42,48-50] As the behaviour of these molecules adsorbed on various substrates has been previously investigated in detail, they may be used as probes of the MCM-41 wall structure. Molecular hydrogen is well characterised both as a bulk solid or liquid[51-54] and as an adsorbate[55-58] and so is used here to probe the channel structure of MCM-41.

The neutron powder diffractometer HIPD at the Intense Pulsed Neutron Source, Argonne National Laboratory (described in Chapter 3) was used for the elastic neutron scattering experiments. A highly ordered MCM-41 sample was used as a substrate. Powder diffraction patterns at 4.2K were measured (with good statistics since subtractions were necessary), at 0, 19.3, 27.2, 34.8 and 50.4 mmol g^{-1}. The latter sample was produced by loading to 50.4 mmol g^{-1} at 21 K and cooling over 30 minutes to 4.2 K. This enabled the excess, unadsorbed hydrogen to first liquefy, and then crystallise, producing a completely loaded sample, with the excess as crystalline solid hydrogen. Although it depends on the temperature, full filling of the space within this MCM-41 was about 40 mmol g^{-1}. Hydrogen and nitrogen isotherms for this MCM-41 material are discussed in Chapter 6, section 6.8. Neutron diffraction patterns at 1.9 K from bare MCM-41 and at various hydrogen loadings are shown in Figure 5.4 below.

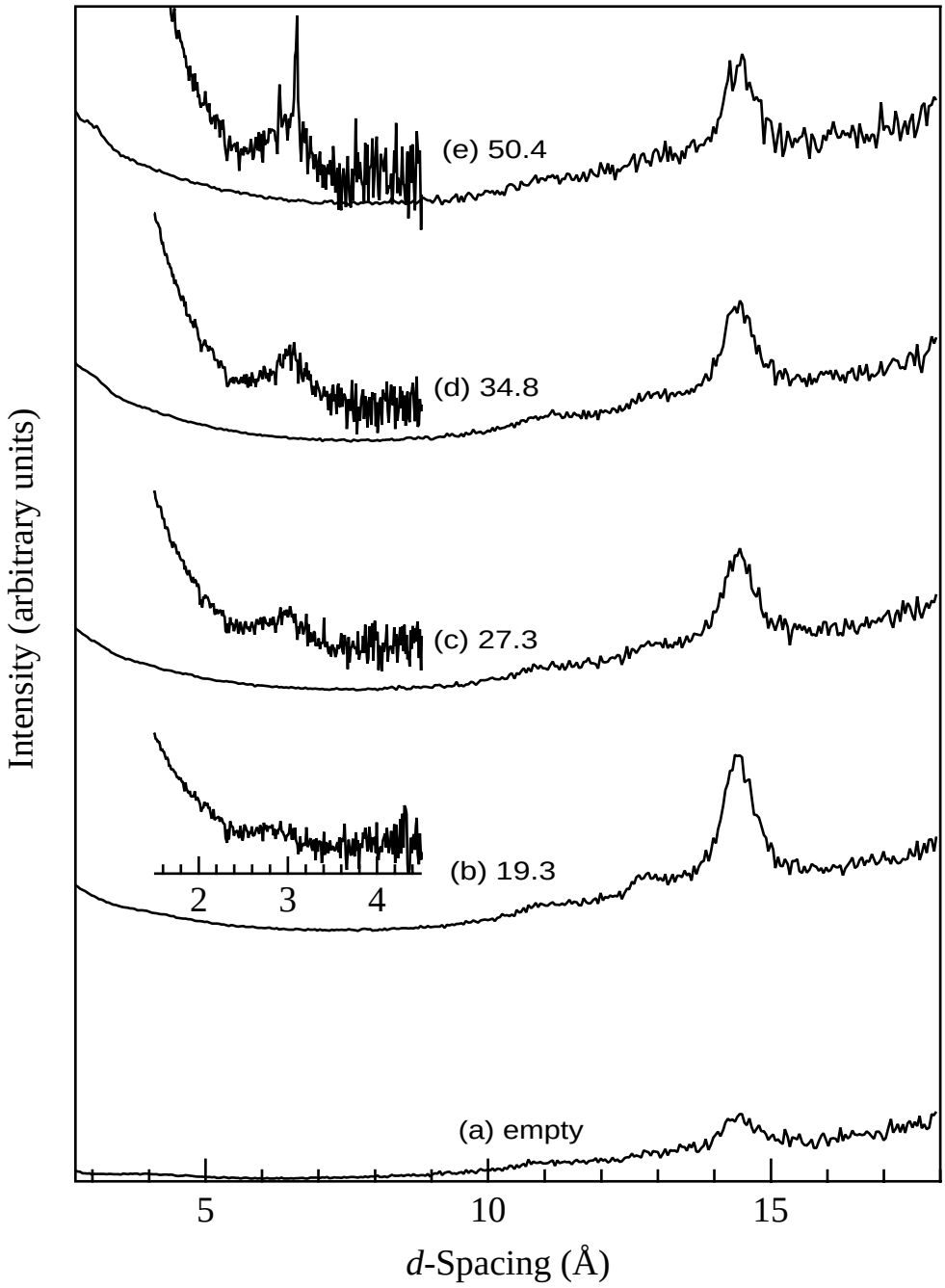

Figure 5.4 *Neutron diffraction pattern from MCM-41, 30˚ counter bank at 1.9 K and various H_2 loadings (mmol g^{-1}) showing the MCM-41 (21) peak. The loadings correspond to 0, 48%, 68%, 87%, and 1.26% of the pore volume filled with hydrogen. The hydrogen peak at ca. 3.1 Å for the same loading is inset.*

5.3.2.2 Unloaded MCM-41

The diffraction pattern from bare, unloaded MCM-41, (Figure 5.4(a)) in both 90˚ and 30˚ counter banks shows the strong scattering from the aluminium can, and weaker scattering from the MCM-41. At lower *d*-spacings the latter is relatively featureless, with only a broad peak stretching from 3 to 5 Å peaking at 4 Å, characteristic of disordered silica materials.[59,60] However at longer *d*-spacings a distinct (21) peak from the hexagonal pore arrangement in the MCM-41 is seen at 14.38(3) Å, with a weaker

peak at 12.8(1) Å from the (30), and at 11.0(2) Å from the unresolved (22) and (31) peaks. The latter are more clearly seen in the 19.3 mmol g^{-1} H_2 loading pattern. These correspond in spacing and intensity to those observed in the X-ray diffraction experiment. The (10), (11) and (20) peaks observed in addition in the X-ray experiment at longer *d*-spacings are out of the wavevector range of HIPD. The observed hexagonal spacing of 38.0 Å is comparable to that observed in the X-ray experiment on freshly prepared calcined samples.

5.3.2.3 Hydrogen Loaded MCM-41

When hydrogen is adsorbed onto the sample three changes to the scattering patterns occur:
(1) Dominating the scattering, a smooth incoherent elastic scattering background from the hydrogen molecules appears, together with, as *d*-spacings decrease, an increasing inelastic intensity in the background, due to the neutron energies becoming sufficient to cause *ortho* to *para* conversion.

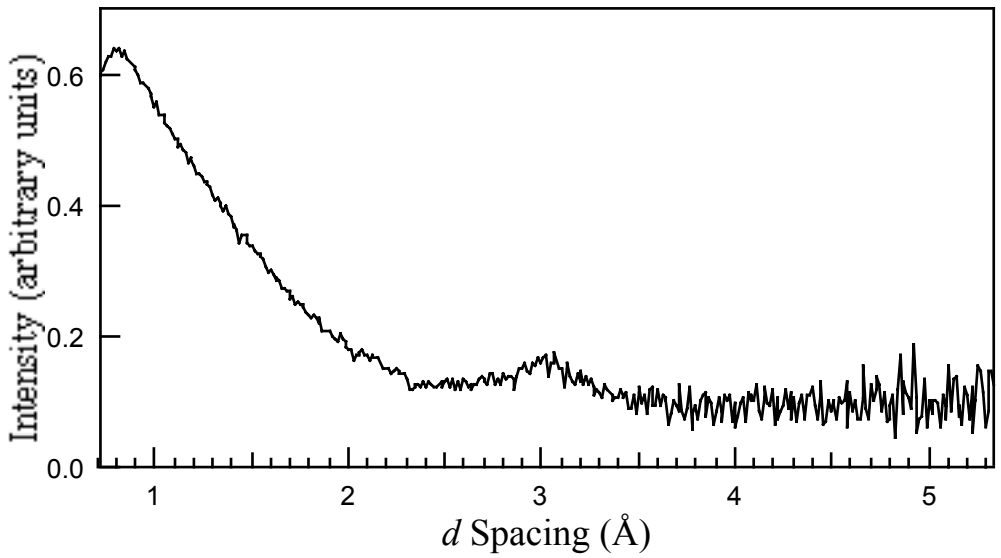

Figure 5.5 *Neutron diffraction pattern from the 90˚ counter bank from 34.8 mmol g^{-1} H_2 on MCM-41 with normalised background from MCM-41 alone subtracted.*

(2) For higher hydrogen loadings a peak at 3.1(1) Å appears. The total scattering, including the peak at 3.1 Å are shown in Figure 5.5. Here, the MCM-41 plus sample container background scattering have been subtracted from a 34.8 mmol g^{-1} H_2 loaded sample at 1.9 K. At the very highest hydrogen loading (50.4 mmol g^{-1}), which is about 20% in excess of the adsorption capacity of the MCM-41 sample, an extra sharp peak at 3.09(1) Å appears in both banks. This is the expected (002) peak from the HCP crystalline phase of H_2 with a unit cell of a= 3.76, c= 6.11 Å previously determined by X-ray diffraction.[51] No other significant crystalline H_2 peaks are observed, again as expected from the X-ray diffraction pattern, where only (002) is strong. This was also the case for hydrogen adsorbed in the pores of vycor glass where higher order peaks were suppressed.[55]

(3) The MCM-41 diffraction peaks, most noticeably the (21), change in intensity, but not in *d*-spacing.

The peak at 3.1 Å for higher hydrogen loadings is relatively broad with a FWHM of about 0.5(1) Å (not as sharp as the H_2 HCP crystalline (002) peak with FWHM of 0.025(5) Å). The position of the peak corresponds to the expected diffraction from H_2-H_2 correlations. In the HCP crystal, the strong peak is observed at 3.09 Å.[51] In a less ordered solid, where a hydrogen molecule is similarly surrounded by hydrogen neighbours, a peak might be expected at a similar position. In an earlier study using methane (discussed in Chapter 6), it was found that the methane within the MCM-41 channels was amorphous as interactions with the silicate walls had prevented crystalline packing. The FWHM of the hydrogen peak observed here (0.5 Å) is that expected from a crystal of size *ca.* 20 Å, which is consistent with possible internal tube diameters in MCM-41. It is thus not possible to distinguish crystalline from amorphous solid hydrogen, especially as local ordering is likely to be similar, and a clear distinction can only be made at longer correlation ranges than 20 Å.

Estimates of the intensity of the 3.1(1) Å peak from both the 30˚ and 90˚ counter banks have been made by subtraction of a linear background. This procedure was also followed for the 50.4 mmol g^{-1} loading where the sharp (002) crystal peak is easily separable from an underlying broader peak. The intensities are shown in Table 5.3, and are normalised to the broad component of the H_2 diffraction for the sample containing 50.4 mmol g^{-1} loading (*ie.* where the MCM-41 pores are saturated). The two counter banks show comparable variation with H_2 loading, though at different Q's, and have been averaged.

Table 5.3 *Relative intensities of the 3.1 Å peak. Note the 50.4 mmol g^{-1} loading includes ca. 20% crystalline H_2 material which is external to the MCM-41 pores.*

Loading	Experiment	Theory
19.3	0.12(6)	0.12
27.2	0.49(5)	0.44
34.8	0.83(5)	0.77
50.4	1	1

Also included in Table 5.3 is a theoretical estimate of the 3.1 Å peak intensity. This is derived by accepting the QENS result (discussed in Chapter 6, section 6.7.1), that there are two distinct types of hydrogen within the MCM-41 pores; a surface adsorbed species whose sites are saturated at a filling of 20 mmol g^{-1}, and a subsequently adsorbed bulk-like species produced by adsorption of a further 20 mmol g^{-1}. It is assumed that the 3.1 Å peak arises only from the two species within the MCM-41 pores (*ie.* not from any external bulk hydrogen), but that the surface adsorbed species has fewer H_2 neighbours. If 1.1 H_2 neighbours for each surface absorbed species is assumed (and 8 for the bulk), the theoretical estimate of intensity shown in Table 5.3 is obtained. This theoretical prediction of the peak intensity agrees well with observation. The estimate of *ca.* one H_2 neighbour for each surface adsorbed dihydrogen molecule is

probably too low because of a greater variability of H_2-H_2 distances at the surface, and should not be taken quantitatively.

The adsorption of H_2 on MCM-41 changes the intensity of the diffraction pattern from the hexagonal patterns of pores in the silica. The (21) peak changes strongly with H_2 loading, increasing in intensity by a factor of three, from zero loading to 19.3 mmol g^{-1}, compared to the unloaded material. Addition of a further 20 mmol g^{-1} then reduces the peak intensity (Table 5.4). The other MCM-41 peaks, although much weaker, go through the same qualitative sequence of intensity change. This pattern of intensity change is not just monotonic and will thus provide a good test of the structural models.

The intensity change of the (21) peak between empty and fully loaded MCM-41 is independent of the detailed structure, and, assuming that all voids are filled with H_2, the relative scattering length densities of crystalline silica and solid hydrogen may be used to predict the intensity ratio of full to empty as 2.3. This is in good agreement with the experiment, indicating that all void space is accessible to H_2. It is at intermediate loadings that differences appear between various possible structural models.

Even though it is at variance with the previously discussed X-ray diffraction results, a fit was attempted to a simple model of a cylindrical, smooth walled tube, in a matrix of relatively dense vacancy-free silica. The relative intensities in two extreme models of hydrogen distribution have been calculated; firstly where the hydrogen is uniformly distributed within the micropore; secondly where the hydrogen sticks to the wall as a skin of density 0.095 g cm^{-3}. Neither model fits the experimental data well, particularly the 19.3 mmol g^{-1} result (Table 5.4). A realistic hydrogen distribution in such a pore may be intermediate, with a density of hydrogen at a minimum in the pore centre, and increasing to the wall. This distribution will give (21) Bragg intensity changes intermediate between the two models. It can be concluded that any reasonable hydrogen distribution in this pore does not fit the neutron diffraction data. Thus the initial assumption about the silica framework is incorrect.

Table 5.4 *Relative intensity of (21) MCM-41 diffraction peak at various H_2 loadings, compared with three models for the system.*

Loading	Experiment	Present Model	Simple Pore Model	
			uniform	skin
0	1	1	1	1
19.3	2.9(3)	2.9	1.57	2.39
27.2	1.9(3)	1.7	1.81	2.84
34.8	2.0(3)	2.1	2.09	1.94
50.4	1.8(4)	2.3	2.3	2.3

When the model proposed from the synchrotron X-ray data from highly ordered MCM-41 (section 5.3.1.2) is used, the neutron results can be reproduced naturally. The silica framework is an inner small diameter cylinder, a larger, void-filled silica framework inside walls which themselves contain voids, though of lesser amount. The adsorbed hydrogen and voids must be partitioned at each loading between the three regions. At lower loadings it is assumed that the central hole is all void, with no hydrogen, in agreement with the isotherm results concerning capillary condensation. The relative Bragg intensities are quite sensitive to the distribution of hydrogen between wall and lining. The observed ratios for 19.3 and 27.2 mmol g^{-1} can be reproduced. In particular the ratio of 2.9 for 19.3 mmol g^{-1} emerges uniquely for a quite reasonable distribution, and the decrease to 2 naturally occurs when a change in loading is made. The model does not even allow that *any* loadings could duplicate both results. The 34.8 mmol g^{-1} data cannot be produced with an empty central core, *all* distributions between wall and lining give ratios of 1 or less. However a 50% loading of the central hole produces a satisfactory fit. At such high overall loadings this loading of the central hole is to be expected, and it is gratifying that the data require it.

Overall the results listed in Table 5.5 suggest a model in which the lining preferentially adsorbs hydrogen and is preferentially saturated. The walls fill at higher loadings and less completely, while the central hole fills last. That is, the lining has a higher surface area and smaller voids (per gram of silica), than the wall.

Table 5.5 *Distribution of volumes ($m^3 \times 10^8$) per gram of MCM-41 under various loadings (mmol g^{-1}) of H_2.*

H_2 Loading	0		19.3	27.2	34.8
Species	silica	void	H_2	H_2	H_2
Central 7 Å Hole	0	11	0	0	6
12.7 Å Lining	25	48	30	38	45
Wall	15	23	10	16	20

5.3.3 SANS Contrast Matching Study

5.3.3.1 Background

Small angle neutron scattering (SANS) provides another test of the proposed model. The contrast match points determined by the contrast variation method are extremely sensitive to the variations in density and template distribution in the silica-organic composite. The SANS contrast variation technique has previously been used for studies of crystallisation and nucleation of zeolites from organic/inorganic composite gels.[61-63] SANS measurements were carried out on MCM-41 synthesis gels at various stages of preparation, as well as on the final calcined products, and the results of these experiments were shown to be are consistent with the model of template and silica distribution described above.

Only a few other SANS studies on MCM-41 and related systems have been published. Firouzi *et al.*[21] report one pattern taken in D_2O of a 1 wt% CTAB solution, with and without dissolved silica, showing the development of a sharp peak due to a hexagonal array of rods from the broad peak characteristic of spherical micelles. Auvray *et al.*[64] published a brief report of a SANS study on the formation of silica gels from TEOS in the presence of n-alkyl ammonium bromide surfactants with different chain lengths. They also show that prior to silicate addition the SANS pattern is typical of disordered isotropic phases containing rod-like micelles. In short chain surfactant systems (C_8 and C_{12}) upon silica gel formation, SANS developed corresponding to a fractal aggregate structure with dimension 1.9. The scattering however, remained dominated by micelle interference peaks indicating a system with short-range order, but no liquid crystal structure. For C_{14}, the development of the hexagonal mesophase during gelation was noted. Finally, a more extensive study has been reported by Glinka *et al.*[65] which also focuses on the synthetic mechanism. They also found that the scattering from calcined samples can be masked by a solution containing 60% D_2O, having the same scattering length density as amorphous silica, and that the calcined samples are fully accessible to water. The power-law scattering for dry calcined materials is reported to have a $Q^{-4.3}$ dependence, characteristic of a rough surface. They found that the masking solutions were not able to penetrate the structure of uncalcined samples, but no further comment on the detailed structure of these materials was made.

A SANS study of the polymerisation of silica in a lamellar mesophase prepared from didodecyldimethylammonium bromide surfactant (DDAB) was carried out by Dubois *et al*.[66] They observed a change in contrast match point between that of a surfactant system containing unpolymerised silica oligomers in the water layers, which scattered in the same way as pure surfactant (contrast match point 4.3 vol% D_2O), and a polymerised silica-surfactant bilayer system, which had a contrast match point of 14 wt% D_2O for a TMOS/water ratio of 10%. From calculations of the contrast match point they showed that most of the silica in the system had condensed onto the DDAB bilayers. From modelling the X-ray diffraction pattern they showed that the polymerisation of silica in the bilayer caused some disruption to the structure which caused a roughening of the bilayer surfaces. This was also observed in electron microscopy. The scale of the disorder was a few times larger than the period of the bilayer, and was attributed to the mechanical tension applied to the silicate polymer by the attraction to the surfactant headgroups. In regions of high silica concentration, surfactant headgroups would be pulled together and cause a curvature of the bilayer surface.

In this work the MCM-41 preparations were made up as described in Chapter 2. Various amounts of purified H_2O and D_2O were used in making up the acidified sodium silicate solutions, and the surfactant template solutions, in order to achieve solutions ranging in D_2O content from 0 mol% to 90 mol% D_2O. Contrast series were prepared for unheated synthesis gels containing 11.5 wt%, 5 wt% and 2 wt% CTAB (as weight percent of the total preparation mass) as well as for a gel containing 4.3 wt% CTAB and 0.2M KBr.

The two different synthesis conditions for MCM-41 were investigated. The first synthesis followed the optimised ordinary synthesis referred to in Chapter 4, based on the initial paper by Beck *et al*.[8] A contrast series of five solutions, having D_2O concentrations of 0, 30, 50, 70, 90 mol% were heated in autoclaves at 100˚C for 3 days, without stirring. The unfiltered wet synthesis gel was run on the SANS machine LOQ, and is hereafter referred to as the "ordinary preparation heated synthesis gel" series. A second ordinary preparation was also made up using this synthesis method. This wet gel was filtered after heating and three dried MCM-41 samples were obtained from it. These were, a filtered sample which still contained excess template (as-prepared), a filtered sample which had been washed three times in hot water to remove excess template, and a calcined sample. These ordinary MCM-41 preparations typically had molar compositions (CTAB 1.00:SiO_2 1.90:Na_2O 0.74:H_2SO_4 0.28:H_2O/D_2O 149). Contrast series on the dried MCM-41 materials were obtained by suspending them in solutions containing D_2O concentrations of 10, 30, 50, 70 and 90 mol%. A dry sample was also run to provide another contrast point, as air has a scattering length density corresponding to 8.9 mol% D_2O. To ensure no air was trapped in the MCM-41 channels, the samples were evacuated before the aqueous solutions were added to the powders. Scattering patterns from these samples at air contrast are shown in Figure 5.6.

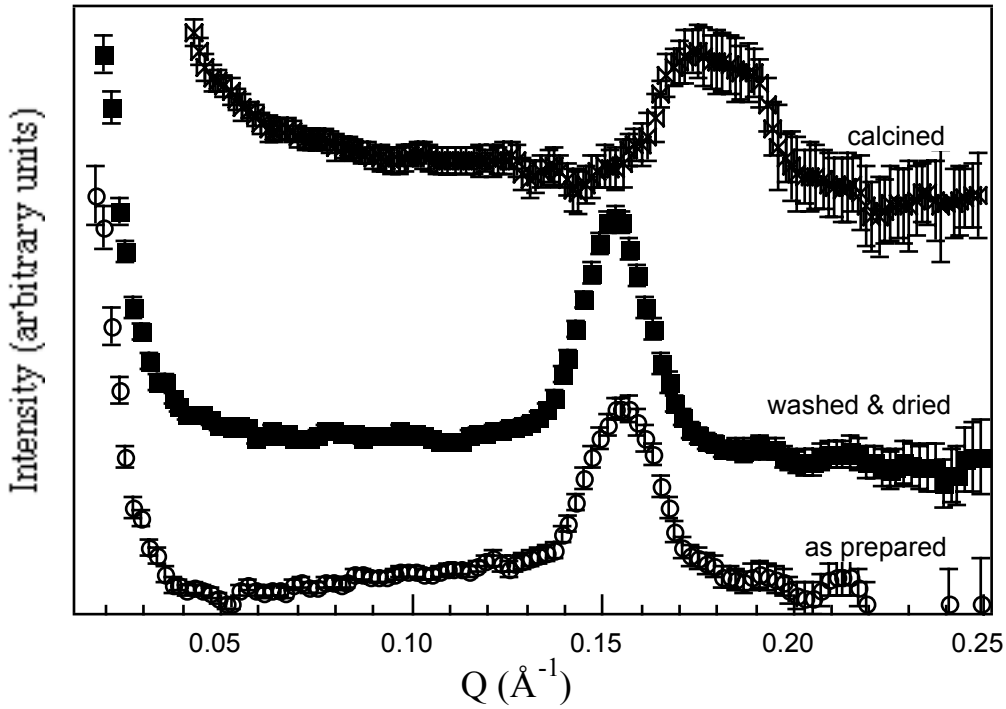

Figure 5.6 *Small angle scattering patterns at air contrast for the as-prepared, washed and calcined samples from the ordinary MCM-41 synthesis.*

The second synthetic method investigated followed the optimised acid-titrated preparation,[67] based on the method published by Ryoo and Kim[33] which results in MCM-41 having a much higher degree of long range order. Using this method a heated synthesis gel contrast series of 0, 30, 50, 70, 90 mol% D_2O was also prepared. In this synthesis, after 24 hours heating of the start gels at 100˚C, each autoclave was cooled to a comfortable handling temperature, opened and a titration performed with one molar acetic acid so as to bring the pH of the whole gel system back to a pH of 11**.** The

autoclaves were then resealed and heated for a further 24 hours and the sequence repeated until 4 days of heating had elapsed. The molar composition of the preparations titrated with acid was typically (CTAB 1.00:SiO_2 2.03:Na_2O 0.79:H_2SO_4 0.27:CH_3COOH 0.45:H_2O/D_2O 173).

As with the ordinary preparation, a second acid-titrated preparation was made up. After filtration and washing with water to remove some of the excess CTAB, this preparation was also divided into several parts. One part was washed with hot water to remove excess CTAB. A second portion was calcined. Small samples of each of the portions of this preparation, and the dried MCM-41 materials from the ordinary preparation were calcined gravimetrically to determine the amount of CTAB remaining in each. The surfactant/silica ratios are shown in Table 5.6. Contrast series of 10, 30, 50, 70, 90 mol% D_2O were run on these materials, with the air contrast used to provide another contrast point. A contrast series was also run, for comparison, on a second washed, dried MCM-41 sample prepared by the acid-titration method, but which used H_2SO_4 as the titrant to maintain a constant pH of 10 during the synthesis, as this had been found to produce material with the greatest degree of long range order. The molar composition of this preparation was (CTAB 1.00:SiO_2 2.08:Na_2O 0.81:H_2SO_4 0.57:H_2O 166).

Table 5.6 *Surfactant/silica ratios for as-prepared, washed and calcined samples from ordinary and acid titrated MCM-41 preparations.*

Sample	Acid Titrated Preparation	Ordinary Preparation
As Prepared	2.68	2.12
Washed	0.93	1.27
Calcined	0	0

5.3.3.2 Particle Surface Structure

Electron microscopy[68] shows that calcined MCM-41 materials contain tactoid-like structures on the scale of microns (see Figure 4.28). Bundles of templated tubes tens of microns long and about a micron across are partially aligned. The origin of the small angle scattering signal is thus an interesting question. One possibility is that only the smallest sizes of the total particle size distribution are sampled in the Q range of the instrument. Another is that the observed scattering comes in part from the scattering length discontinuities at the edges of the tactoids and resembles the "crack scattering" observable for highly crazed solids. To examine these possibilities the power law in the scattering function has been determined for the various gels. Porod's law states that:

$$\ln I \propto -n \ln Q \qquad \textbf{(5.2)}$$

where I is the scattered intensity, Q is momentum transfer and n is the Porod slope, which is related to the nature of the surface of the particles in the scattering medium (see Chapter 3).[34] Porod slopes of 4 indicate that the particles have a smooth surface

with a constant curvature, whereas lesser slopes indicate rougher surfaces. Analysis of Porod plots of the scattering function for the acid titrated, more highly ordered MCM-41 samples at various contrasts shows a set of linear functions with slopes of around 4, (see Table 5.7). This corresponds with that the value of -4.3 found by Glinka *et al.*[65] for a calcined sample at air contrast. The slopes are largely independent of the stage in the synthesis at which the samples were taken. These MCM-41 particles must therefore have a smooth surface at length scales between Q = 0.01 $Å^{-1}$ and Q = 0.06 $Å^{-1}$, over which the power law is obeyed.

At mol% of D_2O close to the contrast match points for these samples, the Porod slopes become lower, around 2.5 to 3. This may indicate a roughness in the surface or an internal structure[69] which is only apparent when the mean density of the particle is matched to the surrounding solution. MCM-41 samples synthesised from the ordinary preparation have lower Porod slopes of around 3 to 3.5 at all contrasts, indicating more inhomogeneity in these samples. Again, close to the contrast match points the slope is lower. In all samples at contrasts close to the match points, as the intensity is close to zero, the effect of noise in the scattering patterns is more apparent, leading to a greater error in estimating the Porod slopes. A set of Porod plots for various contrasts of an ordinary preparation synthesis gel containing 11.5 wt% CTAB is shown in Figure 5.7.

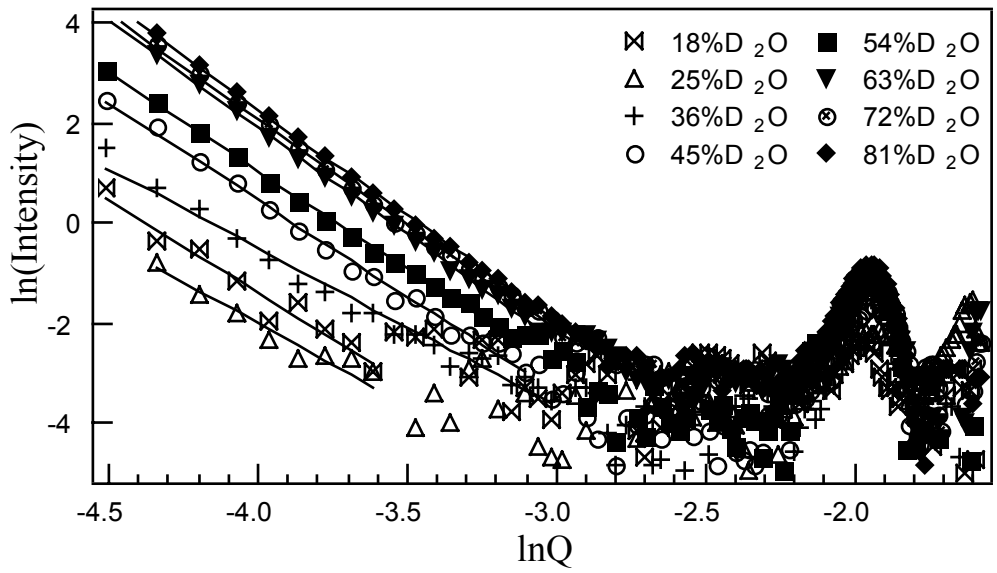

Figure 5.7 *Porod plots of lnI versus lnQ for the contrast series on an unheated MCM-41 synthesis gel containing 11.5 wt% CTAB.*

An estimation of the radii of gyration of particles of all samples by Guinier analysis was attempted but was not successful as the resulting large radii (for instance, 260 Å for a washed, acid titrated sample), indicated that the Guinier approximation (which requires $R_gQ < 1$) was not valid for the minimum Q available, *ca*. 0.006 $Å^{-1}$. This is consistent with evidence from SEM,[68] and from a Scherrer analysis of the peak widths of X-ray diffraction data,[67] which indicate coherence lengths for the hexagonal MCM-41 lattice of the order of 2000 Å.

Table 5.7 *Porod slopes from plots of lnI versus lnQ for MCM-41 samples at various preparation stages.*

Sample	Contrast / mol%D_2O	Acid Preparation	Ordinary Preparation
Heated Synthesis Gel	0	3.9(2)	3.1(2)
	20	3.9(5)	3.7(2)
	40	4.05(6)	4.1(1)
	60	4.08(4)	4.07(4)
	80	3.91(2)	4.08(3)
Washed & Dried	0	4.07(5)	3.13(2)
	10	3.94(4)	2.47(9)
	30	2.5(2)	3.2(2)
	50	3.98(3)	3.21(4)
	70	4.00(4)	3.23(5)
Calcined	8.9	3.72(3)	3.29(3)
	10	3.78(4)	-
	30	3.67(3)	3.11(4)
	50	3.4(1)	2.99(6)
	70	2.9(1)	-
	90	3.56(5)	3.20(4)

Note: - these contrasts were not measured due to restrictions on experimental time.

5.3.3.3 Particle Contrast Match Points

The Porod plots discussed above show that the MCM-41 materials, prepared by the methods described above, obey power law scattering function at low Q. All points on the power law scattering contrast in the same way. Thus it is possible to obtain the scattering length density difference at the interface between particle and solution, through contrast variation plots by selecting a particular Q value, and plotting the square root of the intensity at that value against the concentration of D_2O. A typical example (for the ordinary, unheated synthesis gel containing 11.5 wt% CTAB) is shown in Figure 5.8.

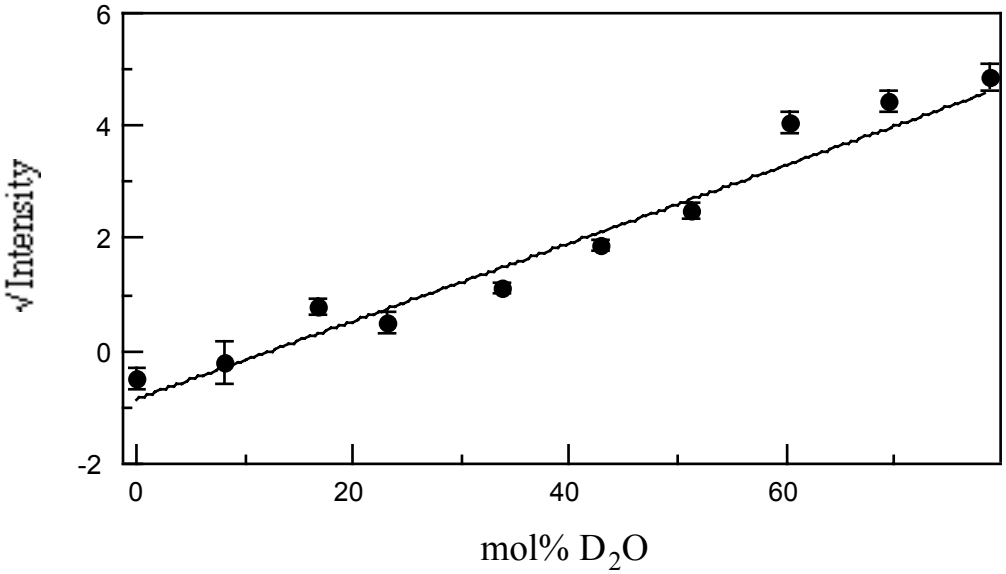

Figure 5.8 *A contrast plot of √I from Porod plots at Q = 0.015 Å^{-1} against mol% D_2O in the solvent mixture of H_2O/D_2O for the synthesis gel sample containing 11.5 wt% CTAB.*

The intensity of the (10) neutron diffraction peak from the hexagonal arrangement of channels was also found to be sensitive to the H_2O/D_2O concentration of the preparation, and for re-wetted, dried samples, also to the composition of the surrounding medium. This indicates some degree of water penetration into the structure, unlike that noted by Glinka *et al.*[65]

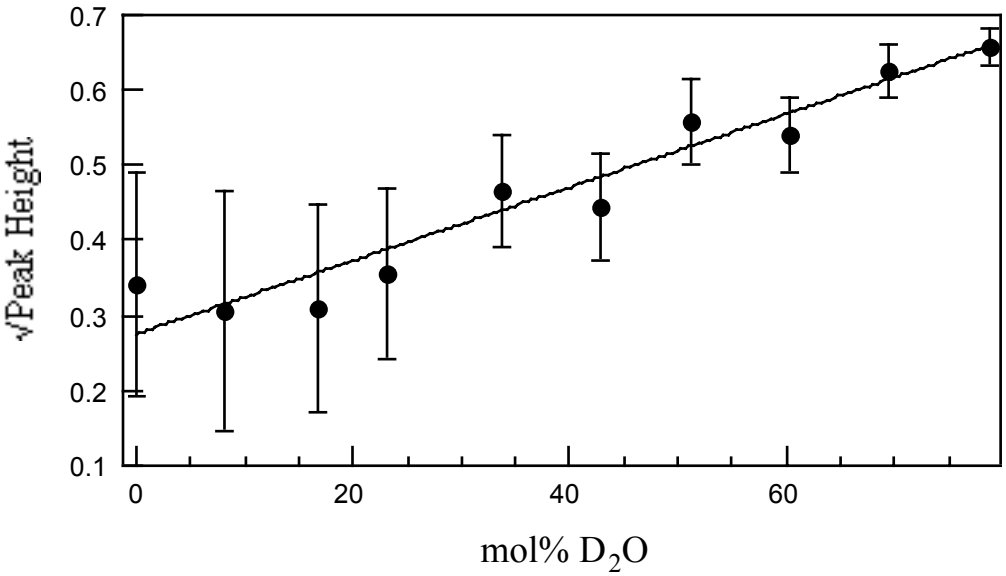

Figure 5.9 *A contrast plot of √Peak Height against mol% D_2O in the solvent mixture of H_2O/D_2O for the synthesis gel containing 11.5 wt% CTAB.*

Contrast match points for the (10) diffraction peak from the hexagonal arrangement of channels were also obtained for all samples. These contrast match points were determined from plots of √(Peak Height) versus mol% D_2O for samples in which a peak was observed. They generally occurred at a different contrast match points to those for

the low Q scattering. A (10) peak height contrast plot is shown in Figure 5.9. The contrast match points for all of the unheated synthesis gels are given in Table 5.8. Those for other heated samples, using both the ordinary and acid titrated MCM-41 synthesis methods, are listed in Table 5.9 below.

The contrast match points at low Q values for all of the ordinary preparation, unheated synthesis gels are low, between 10 and 18 mol% D_2O, indicating the relatively high levels of CTAB in these samples. The trend in the low Q contrast match points measured here, seems to be opposite to that expected. As the CTAB content, with its negative scattering length density, decreases, the low Q contrast match point, considered merely as the sum of components in the system, would be expected to increase, because the remaining components all have positive scattering length densities. This observation is however, probably not significant as the error bars on the low Q contrast match points are large. At present therefore, it is concluded that the synthesis gels have much the same contrast match point with the limits of the experiment.

As the contribution of the CTAB in solution to the scattering length density is also relatively small (-0.244×10^{10} cm^{-2}), while that of the silica is high (3.48×10^{10} cm^{-2}) large changes in CTAB concentration do not much alter the low Q contrast match points. In addition, at 25˚C CTAB is not very soluble in water and is observed to crystallise out of solution, forming large needle-like crystals. These crystals would be too large to contribute to the small angle scattering studied here, and so the scattering from the proportion of CTAB incorporated in such crystals should be ignored, when calculating the expected contrast match points of these solutions. Unfortunately it was impossible to measure the relative amounts of CTAB in the crystals and in the MCM-41 structure.

Table 5.8 *Experimental values for the contrast match points for intensity values at low Q and peak intensities of initial synthesis gels containing various amounts of CTAB. The contrast match points are given as mol% D_2O and the errors given are carried through from the errors from least squares fitting to the data.*

CTAB /wt%	Low Q	(10) Peak
11.5	12(2)	-56(28)
5	10(4)	-52(39)
2	14(5)	-180(47)
4.3+0.2M KBr	18(1)	-

Note: - No peak was observed in this experiment as it was beyond the Q range of the SANS camera.

The structural model proposed in this Chapter for a highly ordered, washed and dried MCM-41 specimen, from an acid titrated preparation, has overall 33 vol% silica and

67 vol% void space. Thus, when the void space in such a sample is completely filled with CTAB, a contrast match point of 22 mol% D_2O is expected, slightly higher than those observed in the synthesis gels. This is probably due to the presence of excess CTAB and the lower degree of silica polymerisation in the walls of these unheated synthesis gels.

In a similar silica-surfactant system containing freshly polymerised silica and DDAB bilayers (10 wt% in water)[66] the peak contrast match point was 12.8 wt% D_2O in a 10% TMOS/water system, in good agreement with the low Q contrast match points found for the MCM-41 synthesis gels, although not with the peak match points found for this hexagonal system. In a 2% TMOS/water - DDAB system, the peak contrast match point was found to be 5.6 wt% D_2O. In that case, calculations showed the contrast match points to correspond to layer of silica condensed next to the surfactant headgroups, or within the bilayers, with the former being regarded as more likely, although the resolution was insufficient to distinguish these. A rise in the scattering at small Q as polymerisation proceeded, which did not contrast at the same point as the diffraction peak, was attributed to the formation of lumps of segregated silica of the order of 1000 Å. The space between bilayers in this lamellar system was 200 Å. Such a large distance between bilayers probably allows the silicate layer to grow from the headgroups into solution, in a manner more akin to ordinary amorphous silica than in MCM-41, where the headgroups of adjacent micelles are close enough to affect the polymerisation of silica polymers on a single micelle.

The synthesis gel containing 4.3 wt% CTAB and 0.2M KBr showed highly unusual behaviour. The small angle X-ray scattering pattern showed a single MCM-41 diffraction peak with broad wings at Q = 0.1394 $Å^{-1}$ which did not change much with aging. The SAXS pattern for the corresponding 5 wt% CTAB synthesis gels, without KBr, always contained several sharp peaks, indicating more long range order. There is clearly some disruption to the formation of an ordered structure caused by the salt. A sample with 11.5 wt% CTAB and 0.4M KBr never developed any hexagonal MCM-41 peaks at all, showing only the lamellar crystalline CTAB peaks.

It is hypothesised that, analogous to the effect of salt on surfactant solutions,[70] the KBr disrupts the formation of a hexagonal structure. The silicated rod-like micelles of CTAB therefore agglomerate into the hexagonal phase in a less ordered fashion than is usual in the unheated synthesis gels. The effect of the added salt is not apparent in the low Q contrast match point. This is much the same as those for the ordinary synthesis gels even though the added salt, with a positive scattering length density, should have pushed the low Q contrast match point higher. The (10) diffraction peak was not, in this case, within the range of the SANS experiment.

The heated synthesis gel samples also have lower contrast match points than expected, perhaps due to the excess CTAB coating the particles. The contrast match point for the ordinary preparation MCM-41 heated synthesis gel is lower than that of the acid-titrated synthesis gel. This may be because it is less crystalline. It shows fewer diffraction peaks in the small angle X-ray scattering (SAXS) pattern, which measures a larger Q range than the SANS machines. Thus heated gels from the ordinary preparation may

contain less polymerised silica in the MCM-41 structure. Also amorphous silica, which precipitates in large particles with sizes beyond the range of the SANS camera, can be neglected for considerations of contrast. SEM micrographs of materials from similar ordinary MCM-41 preparations, included in Chapter 4, show evidence of large silica spheres, which co-exist with the more fibrous material which is believed to be the porous MCM-41.[68] SEM micrographs of the acid titrated preparations, which have much greater long range order (up to 7 peaks visible in the SAXS patterns), show no silica spheres. The effect of removing some of the silica from structures within the range of the SANS camera would be to reduce the low Q contrast match point slightly.

Table 5.9 *Contrast match points for ordinary and acid titrated MCM-41 preparations at various stages of the synthesis. Contrast match points for both intensity values at low Q and peak height are given. Errors are carried through from least squares fitting of the experimental data.*

Preparation Stage	Acid Preparation		Ordinary Preparation	
	Low Q	10 Peak	Low Q	10 Peak
Heated Synthesis Gel	13(1)	-36(20)	9(2)	-120(13)
Filtered & Dried	*	*	19(1)	-90(10)
Washed	22(1)† 28(1)‡	-160(20)† -390(28)‡	19(1)	-100(6)
Calcined	58(2)	61(4)	61(4)	62(6)

Note: * this specimen was not run due to constraints on experimental time.
† from the acetic acid titrated preparation.
‡ from the sulfuric acid titrated preparation.

The low Q contrast match points for the filtered, dried and washed samples, shown in Table 5.9 above, are slightly higher than those of the wet synthesis gels. This is probably due to the removal of a large part of the excess CTAB during the filtration and subsequent washings, and the slight contraction and silica densification of the MCM-41 channel lattice upon drying. X-ray diffraction shows a lattice spacing change from *ca.* 43.5 Å for an ordinary preparation synthesis gel, to 41.4 Å for the dried, uncalcined material from the ordinary preparation, and then to 35.8 Å for calcined materials from the same preparation. This contraction is probably at least partially due to further silica condensation, and physical relaxation as the water is removed and is also observed upon calcination, although to a greater degree. The samples from the acid titrated preparations contract least upon calcination (from *ca.* 43.7 Å wet, to 43.5 Å dried, to 41.6 Å calcined), indicating that the silica lattice is already fairly densely polymerised in the as-synthesised samples. This higher silica density is the likely explanation for the higher contrast match points than for the corresponding ordinary preparation MCM-41 materials at the same preparation stage.

In the calcined materials, for both the ordinary preparation and the acid titrated preparation, the observed contrast match points for both the diffraction peak and low Q scattering are close to those observed and calculated for amorphous colloidal silica, 61-66 wt% D_2O.[61,63] This indicates that the whole framework is permeable to water, as has been found for molecular hydrogen,[44] and that the silica network throughout this framework has approximately the same density as ordinary amorphous colloidal silica. There are very few completely enclosed void spaces in the walls, since this would give lower contrast match points than those observed. Other workers have published helium pycnometry results showing that the skeletal density of the oxide network is equal to that of amorphous silica, 2.2 g cm^{-3},[71] which also indicates the absence of enclosed voids in the walls. Likewise, measurements of the volumes of various liquids adsorbed into boron substituted MCM-41 channels[39] indicated a silica skeletal density of 2.2(1) g cm^{-3}, while the overall density was measured to be 0.97(4) g cm^{-3}, pointing to a low density but completely permeable structure.

5.3.3.4 Particle Internal Structure

The diffraction peak is much more sensitive to the CTAB concentration than the low Q scattering intensity. This can be seen from difference between the absolute intensities of the peak for the calcined and uncalcined samples from the same initial preparation (Figure 5.6). The negative values for the contrast match point of the peak, observed in all uncalcined MCM-41 samples studied, simply means that the contrast match point is never reached (*ie.* it is never possible to add enough H_2O to the silica matrix to match the -0.244×10^{10} cm^{-2} scattering length density of the included CTAB) and is a hypothetical, and unphysical, extrapolation. The trend to more negative values as CTAB is removed however, is of considerable importance in distinguishing possible structures for MCM-41.

The low values of the low Q contrast match points for the unheated synthesis gels, discussed previously, are one indication that a simple model of MCM-41 is not correct. The contrast match points of between 10 and 18 mol% D_2O correspond to volume fractions of between 75% and 90% of holes filled with CTAB of normal density, whereas the simplest model of MCM-41 - CTAB filled tubes of *ca.* 40 Å diameter in a silica matrix with 8 Å walls between tubes - gives a hole volume fraction of only 41%. This simple calculation points to the need for a lower density silica in the walls, thinner walls, high penetrability of the walls by water, or some combination of all three.

From the work discussed above on synchrotron X-ray data[72] on the (h,k) in-plane diffraction from acid titrated samples, a minimum model of MCM-41 was proposed. It required a three region structure; a denser continuous wall region between pores, a shell of less dense silica lining the cylindrical channels and a narrow pore with no silica content. To explain the SANS data, the same three component structural model as proposed in the X-ray work is used. The observed scattering intensities are described in terms of an equation, modified slightly for the neutron case at I(0):

$$I(Q) = ((\Delta\rho_1)A_1 \frac{2J_1(Q,R_1)}{R_1Q} + (\Delta\rho_2)A_2 \frac{2J_1(Q,R_2)}{R_2Q} e^{-\alpha Q^2} + (\Delta\rho_3)A_3 \frac{2J_1(Q,R_3)}{R_3Q})^2 \quad \textbf{(5.3)}$$

where I is the measured intensity, R_1 is the radius of the outer cylinder, R_2 is the radius of the inner cylinder, R_3 is half of the centre to centre distance between the channels (see Figure 5.3) A_1, A_2 and A_3 are the relative areas of each component, $J_1(Q,R_n)$ is the first order Bessel function and α is a Debye-Waller constant. The relative areas, A_1, A_2 and A_3 were taken from the X-ray model, and α was likewise set to 1.0 Å^2. The contrasts, $\Delta\rho_1$, $\Delta\rho_2$, $\Delta\rho_3$ are the differences in scattering length density between the wall and the shell, the shell and the hole, and the wall and the solvent respectively. These were calculated for the empty dry lattice from the silica densities of the X-ray model, and then, given the experimental contrast match points, both for the peak and at low Q values, the amounts of solvent and surfactant in each part of the structure could be calculated.

The extra term of identical form to the first term in equation 5.1 (in the X-ray model above) is necessary at low Q values, in the neutron case, to account for the solvent-wall contrast. This term is required because at, or near I(0) the volume average of the scattering length densities of the various components in the particles (which is the conventional way of determining theoretical contrast match points) must give the same result as the model from the X-ray data. The X-ray equation (5.1) as given is for diffraction. However, at or near I(0) there is also a significant contribution to the scattering from solvent-particle interactions which must be included. The extra term is not necessary in the consideration of the diffraction peak, since it is only the internal density fluctuations which contribute to the intensity of the peak. Because the X-ray model was fitted to data from acid titrated MCM-41 materials only, the calculations were restricted to these materials. As the contrast match points for the ordinary preparation MCM-41 materials are generally similar, the conclusions also hold for these materials. For convenience it is assumed that the partitioning of water into the three components of the structure is isotope independent.

This model worked well for those samples which had been removed from their synthesis liquor, *ie.* those which had been filtered, and/or washed and dried, or calcined. Modelling the calcined sample gave water concentrations filling 100% of all void space in the structure, indicating that the solvent had uniformly penetrated all of the non-silica volume. Attempts in the modelling to fill this void space with any surfactant gave unphysical results.

A fit of the model to data for the washed and dried samples indicated high concentrations of CTAB still present in the void spaces. The washed, acid preparation sample with a contrast match point for the power law region of 22(1) mol% D_2O gave physical values of surfactant and water concentration only when 100% of the central hole was occupied by CTAB, but the wall was *ca.* 8 vol% water/ 52 vol% CTAB/ 40 vol% silica and the lining contained about 1% solvent, being around 64 vol% CTAB/ 35 vol% silica. The sample with a higher power law contrast match point of 28(1) mol% D_2O, indicating less total CTAB present, gave physical values for the full

range of possible concentrations of water and CTAB in the central hole (*ie.* 0-100 vol% water) and between, *ca.* 19-50 vol% water/ 41-10 vol% CTAB/ 40 vol% silica in the denser walls, while the shell contained *ca.* 4-30 vol% water/ 61-35 vol% CTAB/ 35 vol% silica. For water concentrations in the central hole higher than 19%, the walls fill with water preferentially to the lining, so that if the central hole is 100% water, then the void space in the walls are filled with 50 vol% water, and the void spaces in the lining contain only 4 vol% water. Some intermediate situation for example 50 vol% water/ 50 vol% CTAB in the central hole, 35 vol% water/ 25 vol% CTAB/ 40 vol% silica in the walls, and 15 vol% water/ 50 vol% CTAB/ 35 vol% silica in the lining, seems intuitively more realistic.

These values are largely what would be intuitively expected for solvent penetration as the CTAB template is removed from the structure, however it is perhaps surprising that the outer silica wall fills with solvent preferentially to the lining. Possibly this indicates the void spaces present in the wall are smaller, and are positions of higher energy than those of the lining so that as CTAB is washed out of the structure, protruding CTAB molecules retract into a more uniform micellar configuration. That the hole should fill with solvent preferentially to the lining possibly indicates however, that the lining sites are of lower energy to the formation of a self-stabilised micelle within the tube structure. It is likely also, that the surfactant in the walls is, for the most part, comprised of the headgroups with the hydrocarbon tails being more concentrated in the central parts of the micelle. Unfortunately the contrast of the surfactant headgroup (-0.45×10^{10} cm^{-2}) is very similar to that of the tail (-0.46×10^{10} cm^{-2}), so they could not be distinguished in the modelling, given the accuracy of the collected data. Overall, the surprising highly negative extrapolated contrast match points for the diffraction peaks arise quite naturally for differentiated CTAB occupancy of void spaces within the model of MCM-41.

The X-ray model cannot be manipulated by variation of any of the parameters to give results for any of the synthesis gel samples, even the acid titrated heated synthesis gel, which would be expected to be the closest in structure to the dried and calcined materials for which the X-ray model was developed. The presence of unpolymerised silica, and excess CTAB partitioned between the MCM-41 phase, solution, the lamellar CTAB crystalline phase and even large particles of precipitated, amorphous silica create too many variables to allow modelling. The fact that the MCM-41 structure itself may only be partially polymerised in the unheated start gels, and thus has a much lower density than in the heated products, could also contribute.

5.4 Discussion

In the three region model suggested in this Chapter, it is postulated that the denser walls in MCM-41 occur where two cylindrical surfactant micelles, partially covered with silica, have touched and interpenetrated during synthesis. The porous nature of the silicate, however, suggests a significant impact of the surfactant template on the local structure of the silicate, when compared with that of the amorphous silica which forms in this system in the absence of CTAB. In the inner cylinder, closer to the surfactant

headgroups of the micelle template the silicate density is lower, suggesting condensation of the silicate is even less continuous. Previous work has shown the surfactant to have a significant catalytic effect on the silicate polymerisation.[73] Possibly the increase in the reaction rate near the surfactant headgroups is responsible for the growth of an extended, open, kinetically formed network which interpenetrates, as silica coated micelles pack together to form the hexagonal phase crystals. The presence of other anions (*eg.* Br^-, OH^-) in the double layer surrounding the surfactant micelle may also affect the structure of the silicate in this region through steric effects when the anions become trapped by the polymerising silica, interrupting the continuity of the silicate polymerisation.

The surfaces of the micelles may also not be smooth, with some silicate species extending into the interior of the micelle where the hydrocarbon tails of the surfactant are concentrated. Work on pure surfactant systems has shown that water molecules may penetrate the micelle surface to distances of 3-6 carbon atoms,[74] so silicate monomers could also occupy such regions. As long chain silicate polymers form, the neutral silica 'tail' on a growing polymer chain may also be able to preferentially enter the CTAB micelle, as it will be less hydrophilic than the charged silica monomers. However, given the *ca.* 60% reduction in density from pure silica, some type of microstructure in the walls must be inferred, since a purely random creation of voids to this extent would be unlikely to form a stable silica structural framework.

Some form of clathrate structure may be involved in the wall network. Such structures are often proposed as precursors to silicate condensation in zeolites formed with single molecule templates,[75-78] and have even been suggested as MCM-41 precursors.[79] In those cases, the charged silica polyanions cluster around the template molecules, creating a loosely organised silica-organic species. A similar mechanism may operate here, although the supramolecular micelle structure formed by the association of the enclathrated template species obviously disrupts the silica crystallisation into atomically ordered arrays. The low densities indicated by this work may explain why other methods have not shown such small mesopores - in gas adsorption experiments the large amount of void space indicated by the experiments discussed above would merely appear to contribute to the mesopore volume. Previous workers[5,6,26] have implicitly assumed wall densities appropriate for bulk silica giving a much greater mesopore radius.

5.4.1 Other Possible Models for the MCM-41 Structure

Some structural facts about MCM-41 are reviewed:

- There is a hexagonal array of tubes at a spacing of *ca.* 40 Å which are capable of absorbing molecules to at least the size of benzene,[8,80-86] but not much larger (in three dimensions).
- The tubes may be interconnected by pathways capable of supporting bulk hydrogen, so that the void space may be a single space (see Chapter 6, section 6.8).
- Silica densities are everywhere low, less than 50% of cristobalite, even in the so-called walls.

- The projection of the electron density on the hexagonal plane gives a complex pore structure, with a 7 Å radius hole, surrounded by a 12 Å silica lining (of density 35% of bulk silica), with the separating wall 40% of bulk silica density.
- The void space is separated from silica in such a way that when filled with hydrogen, 50% of the hydrogen does not touch silica (see Chapter 6, section 6.7.1).
- When filling with hydrogen the central 7 Å projected void begins filling when the lining and wall are not totally filled, implying that there are voids with radii of *ca.* 7 Å in the lining and wall.
- When sheared, the MCM-41 forming gel, at the CTAB concentrations used here, does *not* decompose into parallel rod-like micelles, but maintains its structure (as discussed in Chapter 4) implying three-dimensional connections between the walls of the pores, and the micelles forming these.

To explain these observations two extreme models may be proposed - if the usual model of an array of large diameter, smooth-walled, non-connected tubes is discounted as not fitting the data listed above at all.

Firstly a model in which the tube is essentially straight and the walls are highly dissected into fibrils and tendrils of silica, with random interconnections between the tubes. That is to say, a model whose structure is random with a short coherence length - the essential structure describable in only ten or twenty Ångstroms of tube length. This model assumes straight, parallel tubes which are not intertwined on length scales of less than hundreds of Ångstroms. Transmission electron micrographs show bends and twists in the channels of MCM-41, but these are on too long a length scale to register in this analysis.[35] In this model, the wall is more massive, while the silica in the linings is more finely divided. This is an entirely reasonable result considering the preparation from the gel.[67] Such a model explains all of the observations, but leaves open the question of what microscopic architecture can stably support the tube network with more than 60% void space, and no micropores.

An alternative is a model in which the free volume is essentially smooth walled, but meanders in some way through the structure. This naturally implies a structural description requiring tens of Ångstroms in size to properly describe the major features. A natural trial model is a defective version of the MCM-48 structure. Intermediate structures between lamellar and hexagonal are commonly discussed,[87] but those between hexagonal and cubic MCM-48 have not been, mainly because the MCM-48 structure itself has only recently been firmly established[88] to be related to that conjectured earlier for corresponding surfactant systems.[70,89-95] A transition of hexagonal phase material to the cubic MCM-48 structure has been recently observed, although the intermediate structure is not discussed.[96] This model of MCM-41 has relatively smooth walled channels, which are largely hexagonally close-packed cylinders, but which have interconnections which resemble pieces of the infinite periodic minimal surface, although much less well ordered than in the material which is normally characterised as MCM-48. Although, considering the method of MCM-41 preparation, this model is considered less likely, it should be considered in more detail.

MCM-48 is a three-dimensionally ordered material of cubic Ia3d symmetry. Although, at the experimental resolutions, a structural description in terms of a network-of-rods model may well be possible, the discussion will concern the infinite periodic minimal surface model. The gyroid minimal surface is of symmetry Ia3d, and such a double sided silica surface of thickness 3-13 Å fits both the available X-ray and TEM data from MCM-48.[88] This structure has infinite helical tubes along {111} and {100} forming two interconnected single voids separated by the minimal surface.

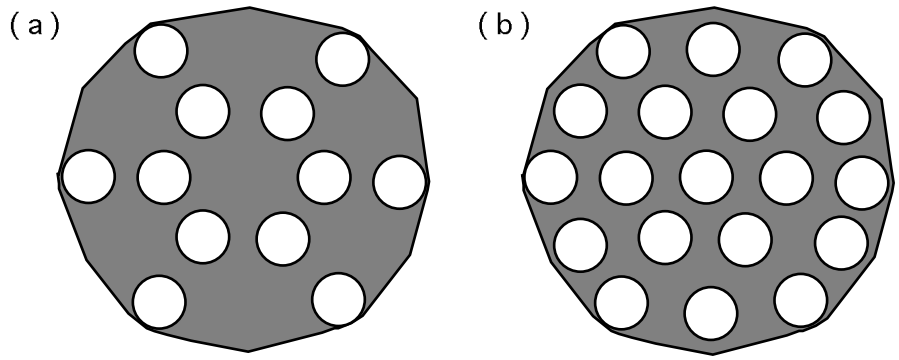

Figure 5.10 *The [111] projections of (a) MCM-48 and (b) MCM-41, showing similarities between these materials - the arrangement of channels is similar, there are merely "missing" channels in the [111] projection of MCM-48.*

To discuss the possible relation to MCM-41, the [111] projection of MCM-48 is considered,[93] the important features of which are shown in Figure 5.10. In this projection it is clear that MCM-41 and MCM-48 may be structurally related. This is already clear from the gross similarity of the X-ray diffraction pattern envelopes of lamellar, hexagonal and cubic phases. MCM-48 has a hexagonal arrangement of tubes along [111] in which one third of the simple hexagonally packed tubes of MCM-41 have been removed. The tube spacing in both MCM-41 and MCM-48 is 45 Å, if typical observed values for unit cells of 45 and 95 Å respectively, are assumed. If a surface thickness of 12 Å in the MCM-48 minimal surface is assumed, then a tube diameter of *ca.* 9 Å along [111] is predicted, surrounded by a lining of thickness 6 Å, at which point the density increases due to the presence of the projection of the minimal surface on the (111) plane. That is, the "wall" region in MCM-41 corresponds to those regions of MCM-48 where the projection of the minimal surface exists. Furthermore, if a mechanism is invoked by which the [111] tubes in MCM-48 can move sideways in (111) by ±[1/3, -1/3, 0], ±[1/3, 0, -1/3] and ±[0, 1/3,-1/3] only, perhaps by some type of stacking fault, then a structure will result in which there is a simple hexagonal lattice of tubes along [111], with no continuous tubes or ordering along the other three body diagonals ([1-11], [-111] and [11-1]). In addition there is a narrow pore in projection, surrounded by a lining, with strong (unshearable) wide pore interconnections between the tubes, a low overall silica density, and smooth walled pores throughout. This seems a reasonable model for MCM-41 consistent with the observations listed above.

It should also be noted that a model proposed for the structure of the related mesoporous silicate, FSM-16, suggests that it may be composed not of long straight channels, but instead contains pores which are likely to be interconnected in a three dimensional network.[18] In that work, this observation is used to distinguish MCM-41

and FSM-16. It may be, however, that the interconnectedness of the pore system is merely a matter of degree, which is dependent upon the synthesis used, and that MCM-41 may therefore also contain connections between channels.

The concentrations of the reagents in the reaction gel used in this work are firmly within the hexagonal, MCM-41 region of the synthesis space.[23] If the MCM-41 and MCM-48 structures are closely related, as proposed above, this suggests a large degree of fuzziness in the definitions of these mesophase surfactant/silica composite structures. Two extreme interpretations of the data are presented here, although many variants and intermediates are equally possible. However, all models *must* satisfy, in particular the detailed data on the projection of the structure on the basal plane presented in this chapter.

5.5 Conclusions

The modelling of the envelope of synchrotron X-ray data from highly crystalline MCM-41 samples shows that these materials have walls made up of silica with variable density regions, not previously suspected. This is modelled as a continuous wall with density much reduced from that of ordinary amorphous silica, and cylinders of less dense material lining the channels created by the dense phase. The completely empty pore space has smaller dimensions than has previously been measured for MCM-41, being only 7 Å in radius, however the 13 Å wide, low density inner lining of the channels will also contain much void space. Even the denser continuous wall structures in this material have been shown to contain void space, which may be responsible for the collective behaviour of gases in MCM-41 (see Chapter 6), since they allow a high degree of connectivity between the pores.

Neutron diffraction patterns show two interesting coherent elastic diffraction features associated with the MCM-41, besides the expected inelastic and incoherent elastic scattering from hydrogen alone (discussed in Chapter 6). There is a peak at 3.1 Å due to H_2-H_2 scattering from bulk hydrogen. The filling dependence of its intensity confirms the inelastic result that the ratio of surface to bulk hydrogen at full filling is 1:1. The second features are MCM-41 diffraction peaks observed at long *d*-spacings (10.7-14.4 Å). The most intense of these, the (21) hexagonal peak, shows dramatic change in intensity of up to a factor of three, as the hydrogen filling is changed. A simple model of MCM-41 of a uniform large mesopore in dense silica does not predict these changes - whether uniform hydrogen filling is assumed, or filling localised to a skin on the mesopore surface, or any intermediate situation. However the more complex “three region” structural model used to fit the synchrotron X-ray data provides an excellent fit. This model has a small empty cylindrical pore, surrounded by a thicker cylindrical lining of silica with some 65 vol% void space. This is in turn surrounded by silica walls which contain 60 vol% void space. This highly porous model fits the (21) diffraction data if hydrogen adsorption is modelled as occurring in three overlapping stages. Initially hydrogen is surface adsorbed in the lining region and fractionally less so in the wall region. Later, the lining pores start to fill up and then the wall pores. Lastly, as the filling of lining and wall becomes almost complete the empty small central pore fills.

The contrast match points from small angle neutron scattering experiments give detailed information about the structure of MCM-41. They indicate that the calcined material is completely penetrable to water, all voids completely filling. Those parts of the structure which are not penetrable, contain silica with the same scattering length density as for amorphous colloidal silica, indicating that the silica structure has much the same density as normal amorphous silica. The contrast match points also indicate that in the uncalcined materials a large part of the wall and shell volume contain CTAB molecules and solvent, and so must be highly porous to account for this. The contrast match points for the synthesis gels reflect the high CTAB concentrations and low degrees of silica polymerisation present in these samples.

These detailed results - bulk properties plus structural data concerning projections onto the MCM-41 basal plane - can be rationalised in two extreme ways. A locally uniform three-dimensional structure can be postulated in which the silica is relatively finely divided into tendrils and sheets with that in the walls being relatively more massive, while the silica in the lining is more finely divided. This means that, proportionately to the total volume in each region, the lining has more surface and the walls more large voids. Thus, considering gas absorption, initially a gas will be adsorbed on the surfaces, and thus be concentrated in the lining. Later the voids will fill, with the largest, the central pore, filling last. Alternatively, at another extreme, a smoother walled mesopore can be imagined which, over longer distances, snakes between hexagonal sites in a way which locally resembles the pore structure of the three-dimensionally ordered structure of MCM-48.

5.6 References

1. O. Franke, G. Schulz-Ekloff, J. Rathousky, J. Stárek and A. Zukal, *J. Chem. Soc., Chem. Commun.,* **1993**, 724-725.
2. P.J. Branton, P.G. Hall and K.S.W. Sing, *J. Chem. Soc., Chem Commun.,* **1993**, 1257-1258.
3. R. Schmidt, M. Stöcker, E. Hansen, D. Akporiaye and O.H. Ellestad, *Microporous Mater.,* **1995**, *3*(4/5), 443-448.
4. P.I. Ravikovitch, S.C.O. Domhnaill, A.V. Neimark, F. Schüth and K.K. Unger, *Langmuir,* **1995**, *11,* 4765-4772.
5. I. Petrovic, A. Navrotsky, C.-Y. Chen and M.E. Davis in *Zeolites and Related Microporous Materials: State of the Art 1994*; Studies in Surface Science and Catalysis, (Eds. J. Weitkamp, H.G. Karge, H. Pfeifer and W. Hölderich), Elsevier Science B.V., Amsterdam, **1994**, *Vol. 84*, 677-684.
6. B.P. Feuston and J.B. Higgins, *J. Phys. Chem.,* **1994**, *98,* 4459-4462.
7. P.J. Branton, P.G. Hall, K.S.W. Sing, H. Reichert, F. Schüth and K.K. Unger, *J. Chem. Soc., Faraday Trans.,* **1994**, *90*(19), 2965-2967.
8. J.S. Beck, J.C. Vartuli, W.J. Roth, M.E. Leonowicz, C.T. Kresge, K.D. Schmitt, C.T.-W. Chu, D.H. Olson, E.W. Sheppard, S.B. McCullen, J.B. Higgins and J.L. Schlenker, *J. Am. Chem. Soc.,* **1992**, *114,* 10834-10843.
9. P.T. Tanev and T.J. Pinnavaia, *Science,* **1995**, *267,* 865-867.

10. Z. Luan, H. He, W. Zhou, C.-F. Cheng and J. Klinowski, *J. Chem. Soc., Faraday Trans.,* **1995**, *91*(17), 2955-2959.
11. S.A. Bagshaw, E. Prouzet and T.J. Pinnavaia, *Science,* **1995**, *269*, 1242-1244.
12. C.Y. Chen, S.L. Burkett, H.-X. Li and M.E. Davis, *Microporous Mater.,* **1993**, *2,* 22.
13. C.-F. Cheng, D.H. Park and J. Klinowski, *J. Chem. Soc., Faraday Trans.,* **1997**, *93*(1), 193-197.
14. C.-F. Cheng, W. Zhou, D.H. Park, J. Klinowski, M. Hargreaves and L.F. Gladden, *J. Chem. Soc., Faraday Trans.,* **1997**, *93*(2), 359-363.
15. P.I. Ravikovitch, D. Wei, W.T. Chueh, G.L. Haller and A.V. Neimark, *J. Phys. Chem. B,* **1997**, *101*(19), 3671-3679.
16. R.K. Iler, *The Chemistry of Silica. Solubility, Polymerization, Colloid and Surface Properties, and Biochemistry*, John Wiley & Sons, New York, **1979**.
17. R. Schmidt, E.W. Hansen, M. Stöcker, D. Akporiaye and O.H. Ellestad, *J. Am. Chem. Soc.,* **1995**, *117,* 4049-4056.
18. C.-Y. Chen, S.-Q. Xiao and M.E. Davis, *Microporous Mater.,* **1995**, *4*(1), 1-20.
19. C.-Y. Chen, H.-X. Li and M.E. Davis, *Microporous Mater.,* **1993**, *2,* 17.
20. K.R. Kloetstra, H.W. Zandbergen, M.A. van Koten and H. van Bekkum, *Catal. Lett.,* **1995**, *33,* 145-156.
21. A. Firouzi, D. Kumar, L.M. Bull, T. Besier, P. Sieger, Q. Huo, S.A. Walker, J.A. Zasadzinski, C. Glinka, J. Nicol, D. Margolese, G.D. Stucky and B.F. Chmelka, *Science,* **1995**, *267*, 1138-1143.
22. M.W. Maddox and K.E. Gubbins, *Int. J. Thermophys.,* **1994**, *15*(6), 1115-1123.
23. G.D. Stucky, A. Monnier, F. Schüth, Q. Huo, D. Margolese, D. Kumar, M. Krishnamurty, P. Petroff, A. Firouzi, M. Janicke and B.F. Chmelka, *Mol. Cryst. Liq. Cryst.,* **1994**, *240,* 187-200.
24. S. Inagaki, Y. Sakamoto, Y. Fukushima and O. Terasaki, *Chem. Mater.,* **1996**, *8*(8), 2089-2095.
25. S. Inagaki, Y. Fukushima, K. Kuroda and K. Kuroda, *J. Colloid Interface Sci.,* **1996**, *180,* 623-624.
26. A. Ortlam, J. Rathousky, G. Schulz-Ekloff and A. Zukal, *Microporous Mater.,* **1996**, *6*(4), 171-180.
27. C.-F. Cheng, H. He, W. Zhou and J. Klinowski, *Chem. Phys. Lett.,* **1995**, *244,* 117-120.
28. Q. Huo, J. Feng, F. Schüth and G.D. Stucky, *Chem. Mater.,* **1997**, *9*(1), 14-17.
29. S. Schacht, Q. Huo, I.G. Voigt-Martin, G.D. Stucky and F. Schüth, *Science,* **1996**, *273*, 768-771.
30. S.A. Davis, S.L. Burkett, N.H. Mendelson and S. Mann, *Nature,* **1997**, *385,* 420-423.
31. G.S. Attard, J.C. Glyde and C.G. Göltner, *Nature,* **1995**, *378*, 366-368.
32. D. Zhao and D. Goldfarb, *J. Chem. Soc., Chem. Commun.,* **1995**, 875-876.
33. R. Ryoo and J.M. Kim, *J. Chem. Soc., Chem. Commun.,* **1995**, *7*, 711-712.
34. O. Glatter and O. Kratky, *Small Angle X-ray Scattering*, Academic Press, London, **1982**, 32-35.
35. V. Alfredsson, M. Keung, A. Monnier, G.D. Stucky, K.K. Unger and F. Schüth, *J. Chem. Soc., Chem. Commun.,* **1994**, 921-922.

36. M.D. Alba, A.I. Becerro and J. Klinowski, *J. Chem. Soc., Faraday Trans.,* **1996**, *92*(5), 849-854.
37. N. Coustel, F. Di Renzo and F. Fajula, *J. Chem. Soc., Chem. Commun.,* **1994**, 967-968.
38. C.J. Plank and L.C. Drake, *J. Colloid Sci.,* **1947**, *2,* 399-412.
39. B. Marler, U. Oberhagemann, S. Vortmann and H. Gies, *Microporous Mater.,* **1996**, *6,* 375-383.
40. D. Khushalani, A. Kuperman, G.A. Ozin, K. Tanaka, J. Garcés, M.M. Olken and N. Coombs, *Adv. Mater.,* **1995**, *7*(10), 842-846.
41. A. Pöppl, M. Hartmann and L. Kevan, *J. Phys. Chem.,* **1995**, *99*(47), 17251-17258.
42. E.W. Hansen, M. Stöcker and R. Schmidt, *J. Phys. Chem.,* **1996**, *100*(6), 2195-2200.
43. K.J. Edler, P.A. Reynolds, F. Trouw and J.W. White, *Chem. Phys. Letters,* **1996**, *249,* 438-443.
44. K.J. Edler, P.A. Reynolds, P.J. Branton, F. Trouw and J.W. White, *J. Chem. Soc., Faraday Trans.,* **1997**, *93*(8), 1667-1674.
45. V.Y. Gusev, X. Feng, Z. Bu, G.L. Haller and J.A. O'Brien, *J. Phys. Chem.,* **1996**, *100*(6), 1985-1988.
46. J. Rathousky, A. Zukal, O. Franke and G. Schulz-Ekloff, *J. Chem. Soc., Faraday Trans.,* **1994**, *90*(18), 2821-2826.
47. J. Rathousky, A. Zukal, O. Franke and G. Schulz-Ekloff, *J. Chem. Soc., Faraday Trans.,* **1995**, *91*(5), 937-940.
48. P.L. Llewellyn, F. Schüth, Y. Grillet, F. Rouquerol and K.K. Unger, *Langmuir,* **1995**, *11,* 574-577.
49. D. Akporaiye, E.W. Hansen, R. Schmidt and M. Stöcker, *J. Phys. Chem.,* **1994**, *98* 1926-1928.
50. S. Komarneni, R. Pidugu and V.C. Menon, *J. Porous Mater.,* **1996**, *3,* 99-106.
51. R.L. Mills and A.F. Schuch, *Phys. Rev. Lett.,* **1965**, *15,* 722-.
52. J.A. Young and J.U. Koppel, *Phys. Rev. 3A,* **1964**, *135*, 603-611.
53. M. Nielsen, *Phys. Rev. B,* **1973**, *7*(4), 1626-1635.
54. W. Langel, D.L. Price, R.O. Simmons and P.E. Sokol, *Phys. Rev. B,* **1988**, *38*(16), 11275-11283.
55. P.E. Sokol, R.T. Azuah, M.R. Gibbs and S.M. Bennington, *J. Low Temp. Phys.,* **1996**, *103*(1/2), 23-33.
56. G.J. Kellogg, J.W. White, K.W. Herwig and P.E. Sokol, *J. Chem. Phys.,* **1990**, *93*(10), 7153-7162.
57. W.J. Stead, P. Meehan and J.W. White, *J. Chem. Soc., Faraday Trans. II,* **1988**, *84*(10), 1655-1668.
58. G.J. Kellogg, P.E. Sokol and J.W. White in *Momentum Distributions*; (Eds. R.N. Silver and P.E. Sokol), Plenum Press, New York & London, **1990**, 351-354
59. H.F. Poulsen, J. Neuefeind, H.-B. Neumann, J.R. Schneider and M.D. Zeidler, *J. Non-Cryst. Solids,* **1995**, *188,* 63-74.
60. A.C. Wright, *J. Non-Cryst. Solids,* **1994**, *179,* 84-115.
61. J. Dougherty, L.E. Iton and J.W. White, *Zeolites,* **1995**, *15,* 640-649.
62. S.L. Suib, *Chem. Rev.,* **1993**, *93*(2), 803-826.

63. L.E. Iton, F. Trouw, T.O. Brun, J.E. Epperson, J.W. White and S.J. Henderson, *Langmuir,* **1992**, *8*(4), 1045-1048.
64. L. Auvray, A. Ayral, T. Dabadie, L. Cot, C. Guizard and J.D.F. Ramsay, *Faraday Discuss.,* **1995**, *101,* 235-247.
65. C.J. Glinka, J.M. Nicol, G.D. Stucky, E. Ramli, D. Margolese, Q. Huo, J.B. Higgins and M.E. Leonowicz, *J. Porous Materials,* **1996**, *3,* 93-98.
66. M. Dubois, T. Gulik-Krzywicki and B. Cabane, *Langmuir,* **1993**, *9*(3), 673-680.
67. K.J. Edler and J.W. White, *Chem. Mater.,* **1997**, *9*(5), 1226-1233.
68. K.J. Edler, J. Dougherty, R. Durand, L. Iton, G. Kirton, G. Lockhart, Z. Wang, R. Withers and J.W. White, *Colloids Surfaces A,* **1995**, *102,* 213-230.
69. B. Jacrot, *Rep. Prog. Phys.,* **1976**, *39,* 911-953.
70. G.J.T. Tiddy, *Physics Reports,* **1980**, *57*(1), 1-46.
71. T. Dabadie, A. Ayral, C. Guizard, L. Cot and P. Lacan, *J. Mater. Chem.,* **1996**, *6*(11), 1789-1794.
72. K.J. Edler, P.A. Reynolds, J.W. White and D. Cookson, *J. Chem. Soc., Faraday Trans.,* **1997**, *93*(1), 199-202.
73. C.-F. Cheng, Z. Luan and J. Klinowski, *Langmuir,* **1995**, *11,* 2815-2819.
74. J.H. Fendler and E.J. Fendler, *Catalysis in Micellar and Macromolecular Systems*, Academic Press, New York, **1975**.
75. S.L. Burkett and M.E. Davis, *J. Phys. Chem.,* **1994**, *98*(17), 4647-4653.
76. W.M. Hendricks, A.T. Bell and C.J. Radke, *J. Phys. Chem.,* **1991**, *95*(23), 9513-9518.
77. C.T.G. Knight, *Zeolites,* **1990**, *10,* 140-144.
78. S.L. Burkett and M.E. Davis, *Chem. Mater.,* **1995**, *7*(5), 920-928.
79. J. Emmer and M. Wiebcke, *J. Chem. Soc., Chem. Commun.,* **1994**, 2079-2080.
80. E. Armengol, M.L. Cano, A. Corma, H. Garcia and M.T. Navarro, *J. Chem. Soc., Chem. Commun.,* **1995**, 519-520.
81. K.M. Reddy, I. Moudrakovski and A. Sayari, *J. Chem. Soc., Chem. Commun.,* **1994**, 1059-1060.
82. K.R. Kloetstra and H. van Bekkum, *J. Chem. Soc., Chem. Commun.,* **1995**, 1005-1006.
83. A. Corma, V. Fornés, H. García, M.A. Miranda and M.J. Sabater, *J. Am. Chem. Soc.,* **1994**, *116*(21), 9767-9768.
84. J. Aguado, D.P. Serrano, M.D. Romero and J.M. Escola, *J. Chem. Soc., Chem. Commun.,* **1996**, 725-726.
85. T. Blasco, A. Corma, M.T. Navarro and J. Pérez Pariente, *J. Catal.,* **1995**, *156,* 65-74.
86. R. Netrabukkana, K. Lourvanij and G.L. Rorrer, *Ind. Eng. Chem. Res.,* **1996**, *35*(2), 458-464.
87. A. Monnier, F. Schüth, Q. Huo, D. Kumar, D. Margolese, R.S. Maxwell, G.D. Stucky, M. Krishnamurty, P. Petroff, A. Firouzi, M. Janicke and B.F. Chmelka, *Science,* **1993**, *261*, 1299-1303.
88. V. Alfredsson and M.W. Anderson, *Chem. Mater.,* **1996**, *8*(5), 1141-1146.
89. V. Luzzati, A. Tardieu, T. Gulik-Krzywicki, E. Rivas and F. Reiss-Husson, *Nature,* **1968**, *220,* 485.
90. K. Fontell, *Colloid and Polymer Sci.,* **1972**, *43,* 156.
91. K. Fontell, *Colloid and Polymer. Sci.,* **1990**, *268,* 264.

92. K. Fontell, *Adv. Colloid and Inter. Sci.,* **1992**, *41,* 127.
93. L. Larsson, *J. Phys. Chem.,* **1989**, *93,* 7304.
94. P. Ekwall, L. Mandell and K. Fontell, *J. Colloid and Inter. Sci.,* **1969**, *29,* 639.
95. J. Charvolin and J.F. Sadoc, *Colloid and Polymer Sci.,* **1990**, *268,* 190.
96. Q. Huo, D.I. Margolese and G.D. Stucky, *Chem. Mater.,* **1996**, *8*(5), 1147-1160.